# NEAR-INFRARED QUANTITATIVE PHASE IMAGING OF CELLULAR MANIPULATION UNDER DIFFERENT PHYSIO-CHEMICAL ENVIRONMENTS

by

BIPIN JOSHI

Presented to the Faculty of the Graduate School of
The University of Texas at Arlington in Partial Fulfillment
of the Requirements
for the Degree of

MASTER OF SCIENCE IN BIOENGINEERING

THE UNIVERSITY OF TEXAS AT ARLINGTON

December 2012

Acknowledgements

When I joined University of Texas at Arlington as a graduate student in the department of Bioengineering, I always had a dream to work in the diverse field of optics that could possibly be applied in the field of medicine. Dr. Mohanty's lab of biophysics exactly did the trick. I would like to take this opportunity to thank my supervisor Dr. Samarendra Mohanty for believing in me and giving me an opportunity to work with him in the area of optics as well as in biophysics. I could relate my knowledge that I had gained all these years to experiments being performed in his lab. He is a motivation to me and will always be in my future career. His hard work and sheer interest in research motivated me to grow and learn more in the field of optics and persuaded me to develop into a research oriented person.

I would also like to thank Dr. Ling Gu, Nelson and my other lab members who have always helped me in making this thesis a success. Dr. Gu was always supportive and taught me working with cells and cell culturing -an important part in planning out any experiment. Nelson, my lab mate was always available in person or over phone to give technical solutions over problems that I faced in my early stages while performing experiments. All my other lab members always helped me whenever I needed them the most.

Most of all, I would like to dedicate this thesis as a small effort to give a pleasant memory to my family. They made this world a beautiful place to live in and to enjoy as well. Without their support I don't think I would have come to this point. They have supported and encouraged me for over 24 years now. It is because of all their support, motivation and belief in me that I could successfully complete my masters in Bioengineering. I would thus take this opportunity to give all the credits in making this thesis possible to my mom (Mrs. Jyoti Joshi), my dad (Mr. Shamkant Joshi) and my sister

(Neha). This wouldn't have been possible without their strong support and encouragement.

I would also like to thank all my friends who were an integral part of my life here at UT Arlington. They all have helped me in some way or the other to make this thesis successful. Thank you all for believing and encouraging me.

November 20, 2012

Abstract

NEAR-INFRARED QUANTITATIVE PHASE IMAGING OF CELLULAR MANIPULATION UNDER DIFFERENT PHYSIO-CHEMICAL ENVIRONMENTS

Bipin Joshi, MS

The University of Texas at Arlington, 2012

Supervising Professor: Samarendra Mohanty

Quantitative phase imaging using Digital Holographic Microscopy (DHM) is emerging as a label-free and wide-field method of characterizing cells with high spatio-temporal resolution. In parallel, silicon based micromechanical and electronic devices are allowing both manipulation (e.g. electrical stimulation, mechanical actuation) as well as characterization (electrical and mechanical) of micro and nano-scopic samples. This has revolutionized development of lab-on-a-chip devices for high throughput analysis of cells and molecules for diagnosis of disease and screening of drug-effects. However, very little progress has been made in optical (e.g. fluorescence, Raman etc) characterization of samples on these silicon-based devices. Especially, wide-field high-resolution optical imaging and characterization of samples under silicon environment has not been possible owing to the opacity of silicon to visible light. This thesis reports high resolution near-infrared quantitative phase imaging of cells through silicon, in isotonic as well as hypotonic environment using DHM.

Further, several microscopic (AFM, laser manipulation) methods are being developed for characterization of mechanical properties (e.g. elasticity) of cells so as to determine changes during physiological stress. In particular, optical tweezers are used

for transverse-stretching cells by actuating anchored-beads as handles and imaging using phase-contrast microscopy. While this method is constantly gaining more attention due to non-contact nature of actuation, it is very time consuming and has low working distance. The thesis describes development of a weakly-focused laser beam for axial-stretching of cell by scattering force, which can be easily extended for wide-area stretching. Application of DHM allowed cell imaging with nm-resolution when stretched axially. Development of an empirical formula for force exerted by defocused light beam on cell surface led to measurement of elastic property of cell. In addition to this, the thesis aimed at evaluating changes in elastic properties of cell under over-expression of certain proteins (HOX-B9), which is believed to be involved in tumorigenesis. Significant reduction in elastic property of cells over-expressing HOXB9 was found as compared to the control cells. Thus, the thesis paves the way for development of a method for optical manipulation and imaging of cells for characterization of their elastic properties in different physiological states, and probe nanoscale interactions with different physio-chemical agents in a non-invasive and label-free manner.

Table of Contents

List of Illustrations

List of Tables

# Chapter 1

## Introduction

This thesis discusses about “Digital Holographic Microscopy”- an imaging methodology which can detect nanometer level of changes and some of its applications in the vast and growing field of Biophysics. Chapters in this thesis describe working principle of Digital Holographic Microscopy (DHM), its reconstruction techniques as well as cell manipulation imaging in detail. Although Digital holographic microscopy is a widely known technique to characterize cellular level changes, set up used in this thesis uses common path technique in accordance with off axis holography and spatial filtering which requires better and thorough understanding. Chapter 1 talks about background of microscopy and need of DHM. Later half of Chapter 1 explains working principle of DHM thoroughly. Chapter 2 discusses an innovative technique of imaging through silicon wafer using DHM and its validation on human cells. Moreover it demonstrates cellular level changes when cells are stimulated. Chapter 3 enlightens the difference between normal and diseased cells by optically stretching them and imaging them using DHM at the same time. DHM is truly an innovative tool to explore nanometer level changes for structural and functional cellular investigations.

## 1.1 Motivation

History of microscopes shows that there was a clear need of a device that could see cells which are normally transparent under normal light microscope. Much of research has been done in this area to make images look better by enhancing the contrast of cells. Few methods include applying dyes. However dyes were tested to be poisonous to cells and would damage the cells if kept for long time. Other methods gave pretty decent images but lacked quantitative information of cells. Advances in microscopy have discovered DHM which has evolved as an innovative technique to characterize

quantitative information of samples. In this era science has grown to its peak. Silicon chip is used to achieve more precise and faster results in the area of medicine. Great researches have been going on silicon. Few of them include use of silicon chip to control cell-cell interactions micromechanically, designing silicon nanoparticles for in vivo and in vitro applications, cellular interactions of surface modified nanoporous silicon particles etc. It is therefore necessary to image cells under silicon and characterize cellular activity that cannot be seen otherwise. Although much work has been done in the area of DHM, currently there exists no such technique that can see through silicon and give quantitative information of cells laid under silicon. DHM in accordance with Near Infrared light can be used to see through silicon and get quantitative information of samples.

The worst health crisis that world is facing in this era is cancer. American Cancer Society® has reported an estimated number of 1,638,910 new cases of cancer just for the year of 2012 in USA. Over 12.7 million new cases of cancer were diagnosed in the entire world in the year 2008 as reported by Cancer research UK. To allow better understanding of root cause of cancer, quantitative information on cancer cells is necessary. DHM on cells which over-express a protein is performed in this thesis to examine what might be one of the potential contributors towards cancer.

## 1.2 Background

During the era of Renaissance, light microscope was invented that helped investigating tiny particles [1]. A light microscope which is a device that made us possible to see enlarged version of minuscule objects through a combination of lenses is a remarkable discovery of all the times. Entire world has seen major advancements in microscopy since then, until the mid $19^{th}$ century in which one of the greatest and finest advancement in the field of light microscopy took place [2]. Charles Spencer, an American businessman built one of the finest light microscope of the era that could

enlarge small scaled objects to a much bigger scale. A large amount of efforts have been committed towards obtaining better resolution and enhanced contrast of the image in microscopy since then [2]. Just when these important advancements were being discovered, Abbe proved that the ultimate resolution that one can go up to with light microscope even with ideal lenses and perfect illumination is half the wavelength of light [4]. Thus there was a limitation on distinguishing objects smaller than half the wavelength of light. Any two lines closer than this distance would appear as a single line and any object smaller than this distance would not appear at all or at most would appear blurred. This obstacle was surpassed by the invention of an electron microscope. The electron microscope incorporates high velocity electrons in vacuum so that their wavelengths are exceptionally small [5]. These small wavelengths enabled visualizing smaller particles which were difficult to see earlier. The image would form on electron sensitive photographic plate for an electron microscope. The electron microscope suffered from a severe drawback though. Since all the living samples are not compatible to high vacuum it incorporates, the electron microscope cannot be used to image living cells or tissues. To contrary, light microscopes enabled the user to image and characterize live cells and study their behavior.

The major challenge for light microscope is to improve contrast between cells and their surroundings. A cell is a transparent object having weak endogenous absorption and low scattering properties making them optically semi-transparent when imaged under bright light. This optical transparency of label free live biological specimen limits the extraction of information from bright field microscopic images because these specimens generally lack visible amplitude modulating components thus generating low contrast. Contrast can be differentiated as endogenous and exogenous. Endogenous is intrinsic kind of contrast usually generated by structures present inside the specimen.

Exogenous contrast is a contrast obtained by affixing a contrast agent onto the specimen or to a structure inside the specimen. A contrast agent can be a dye or a stain. A perfect example of exogenous dye is GFP (Green Fluorescent Protein). Nowadays living cells are genetically modified to express GFP thus changing exogenous contrast into endogenous one [6]. Even with these contrast agents, deep tissue imaging is difficult. This issue has been overcome by scientists over time by using noble techniques such as Optical Coherence Tomography (OCT) [6], Confocal microscopy [8] etc.

### 1.3 Light propagation and phase change

Contrast of the imaging sample is important. A good contrast between a cell sample and its surrounding is necessary to observe the sample precisely. When a light passes through a stained sample, some of the light is absorbed by the localized pigments thus changing the amplitude of the light coming out from that area [3]. This is perceived by a human eye as change in brightness and color with respect to the background. If all the light is passing through the cell then the cell would look transparent. In which case, a human eye would not be able to see the cell in visible range. Zernike proved that cells do affect the optical phase of the light passing through them as shown in figure 1-1. He showed that although cells are optically transparent under bright light, they affect the wavefront of light passing through it because of different refractive index across the cell. This is because light travels with different speed in different refractive index medium thus experiencing different time delay across the cell. Waves passing through the thicker and higher refractive index area of the cell will experience higher phase lag as compared to the waves passing through thinner and lower refractive index area. Visualization of this phase modulation that occurs when light traverses through a transparent cell, could provide essential information about the cell and its components. Zernike later developed

a method in which phase information of unstained cells is used to create high contrast images which we now know as phase contrast microscopy.

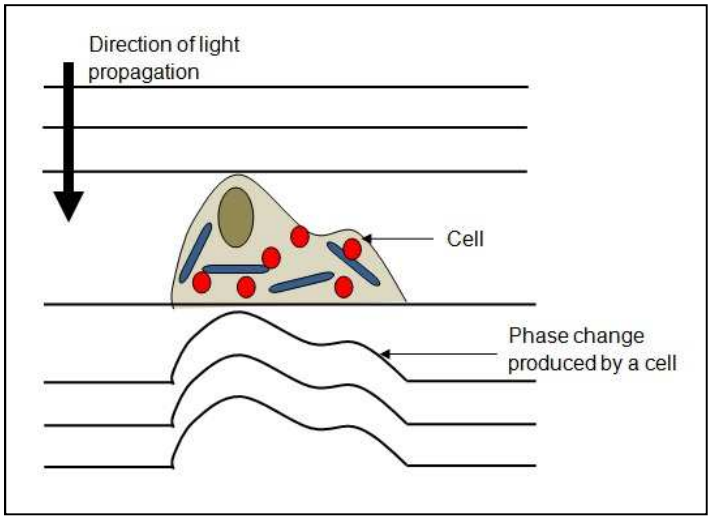


Figure 1-1: Propagation of light wavefronts through a cell shown by an arrow. Propagation of light through a cell induces time lag due to varied refractive index and thickness across the cell thus inducing phase change.

## 1.3 Microscopy Techniques

### *1.3.1 Phase Contrast Microscopy*

The phase contrast microscopy uses a phase plate and a phase annulus to increase the contrast. This is done by converting the phase lag induced by a cell into amplitude variation so as to perceive the images as change in brightness and thus getting higher contrast. The light is passed through a phase annulus so that light coming out from the condenser is a hollow cone which is concentrated onto a phase sample. Let us consider light coming out from the sample is out of phase by 90º (λ/4). This out of phase light is collected by a microscopic objective and is focused onto imaging plane.

The light which is unperturbed by the phase object is passed through a phase ring and is advanced by 90º (λ/4). This result in destructive interference of light converting phase difference into amplitude differences observed as intensity contrast [10]. It allows us to see details of normally transparent cells relatively darker than the background. Phase lag is dependent on the refractive index and thickness of the specimen.

Phase contrast microscopy suffered from a major disadvantage of light halos around the cells [9]. Phase shift gradient is greatest at the boundary of the cell resulting into blurred edges. This causes problems when there is a demand of calculating cell size or investigating a cell structure.

*1.3.2 Differential interference Contrast Microscopy (DIC)*

George Nomarski invented Differential interference contrast microscopy that uses the same principle of Phase contrast microscopy that is using the phase of the object to perceive it as intensity contrast. DIC does not use phase plate as in traditional phase contrast microscope. Instead it uses Nomarski-modified Wollaston prism to get two rays of different polarization [11]. With a help of a condenser, light is concentrated on to the sample. These rays pass through the sample very small distance apart from each other. Refractive index materials inside the cell makes one ray out of phase compared to other one. Since two light rays hitting the sample are at different polarization, they do not interfere in the sample. Rays coming out from the sample are acquired by a microscopic objective and are passed through another Nomarski-modified Wollaston prism where they recombine having same polarity. As the path travelled by two rays are slightly off with respect to each other, interference between them results in difference in intensity which is perceived as better contrast.

Although DIC microscopy completely eliminates halo effects as in Phase contrast microscopy, it is very expensive to build because of the cost of individual components. Moreover it requires considerable increase in the incident light power for imaging.

*1.3.3 Hoffman Modulation Contrast Microscopy (HMC)*

Hoffman modulation contrast microscopy was invented by Robert Hoffman in the year 1975 [12][13]. This is yet another technique by which nearly transparent specimens can be viewed. Hoffman Modulation contrast microscopy emphasizes on phase gradients within the sample and displays them as varied brightened or darkened areas. A modulator is used to accomplish this task. A modulator with three regions of different attenuation regions usually T(Transmission)=100%, 15% and 1% is placed in the back focal plane of a microscopic objective. A slit is placed in front of a condenser in such a way that light passing through slit is incident on 15% region of the modulator. In the sample where there is high change in refractive index, light will refract and thus will change its path. The light which does not experience any refraction will pass through middle region of 15% thus giving an image gray background. Light which experiences refraction will have either positive or negative gradient in the Fourier plane of the microscopic objective. These rays pass through 1% or 100% region of modulator giving an image with varied gray levels.

Although Hoffman modulation contrast microscopy gives a 3D view of a sample, it is not suited for localization of details inside a specimen at depths. Similar to DIC, HMC also has expensive optical components which make it costly to implement.

## 1.4 Digital Holographic Microscopy (DHM)

Phase contrast microscopy, Differential interference contrast microscopy and Hoffman Modulation contrast microscopy are developed to transform phase information of a cell into amplitude or brightness information to get better contrast and are useful in

many areas of cellular studies. These imaging techniques can provide only the qualitative information about a cell [14]. Scientists have been working on to get the quantitative information such as refractive index, dry mass, shape, thickness and volume of a cell. This search has resulted in an innovation of interferometric quantitative microscopy technique which uses a coherent light and phase of the specimen to calculate quantitative results. This microscopy technique uses a computation approach to phase information that provides mathematically derived information about phase modulating characters [15][16]. In all other traditional microscopy techniques, amplitude and phase information of a specimen is intrinsically blended in with each other and are not possible to separate. With the help of DHM, it is possible to distinguish as well as separate amplitude information and phase information of a cell or any other specimen. The amplitude image is similar to bright field image captured by an ordinary microscope. DHM is a very sensitive microscopy technique having resolution in the orders of nanometers [19]. DHM has an added advantage that all the cells that are studied are always in focus and the images can be reconstructed many times by readjusting the focus to find the best position. Cells images can be presented as normal 2D as well as in 3D.

Digital holographic microscopy can be used in reflection mode [17] or as most commonly used for cell studies in transmission mode to image normally transparent cells [18]. System used here is derived from Mach-Zehnder interferometer that uses off axis holography technique. Off axis holography includes object beam and reference beam interfering at an angle to produce interference fringes. The images are reconstructed numerically by using Fresnel diffraction theory. Quantitative phase map contains all the information about refractive index, thickness, volume of a cell. This makes it a valuable tool for structural and functional biological specimen examinations. Quantitative phase microscopy has been used towards many different applications. Few of them include

assessment of cellular morphology [20], study of mammalian cells [18] animal and fish cells [21] and cell proliferation, cell movement [22].

Table 1-1 Comparison of different microscopy techniques for live cell imaging

| Method | Advantages | Limitations | Resolution | Applications |
|---|---|---|---|---|
| Phase Contrast Microscopy | High Contrast Images | Blurred edges and light halos, can't give quantitative information of sample | Poor | Qualitative live cell imaging |
| Differential Interference Contrast | No blurred edges or light halos | Costly and shadow effect, can't give quantitative information of sample | Low | Qualitative live cell imaging |
| Hoffman Modulation Contrast | Gives 3D view of sample | Can't give localization details inside the sample and quantitative information of sample | Sub-micrometer | Qualitative live cell imaging |
| Digital Holographic Microscopy | Gives quantitative information such as refractive index, thickness of the sample | Samples having same refractive index that of surrounding medium cannot be distinguished | Angstrom | Quantitative imaging of live cells |

## 1.5 Experimental Setup

Figure 1-2 shows experimental setup for Digital Holographic Microscopy. The digital holographic microscopy uses a common path interferometric technique. The condenser lens illuminates the sample by concentrating the laser on the X-Y-Z sample stage. Light passing through the sample is collected by a microscopic objective (40X or 100X). Beam splitter 1 splits the beam coming out from microscopic objective into two beams. The object beam (O) is allowed to fall on beam combiner (BS2). Another beam coming out

from beam splitter 1 is tightly focused onto a pinhole of 25µm diameter for spatially filtering the beam. Spatial filtration removes phase information and intensity information carried by the beam. This is called as a reference beam (R). Reference beam coming out from the pinhole is allowed to interfere with object beam (O) into a beam combiner (BS1). This interference between object beam (O) and reference beam (R) causes interference pattern of dark and white bands which is projected on a CMOS camera capturing pictures at a rate of 25fps (DCC1545M, Thorlabs Inc).

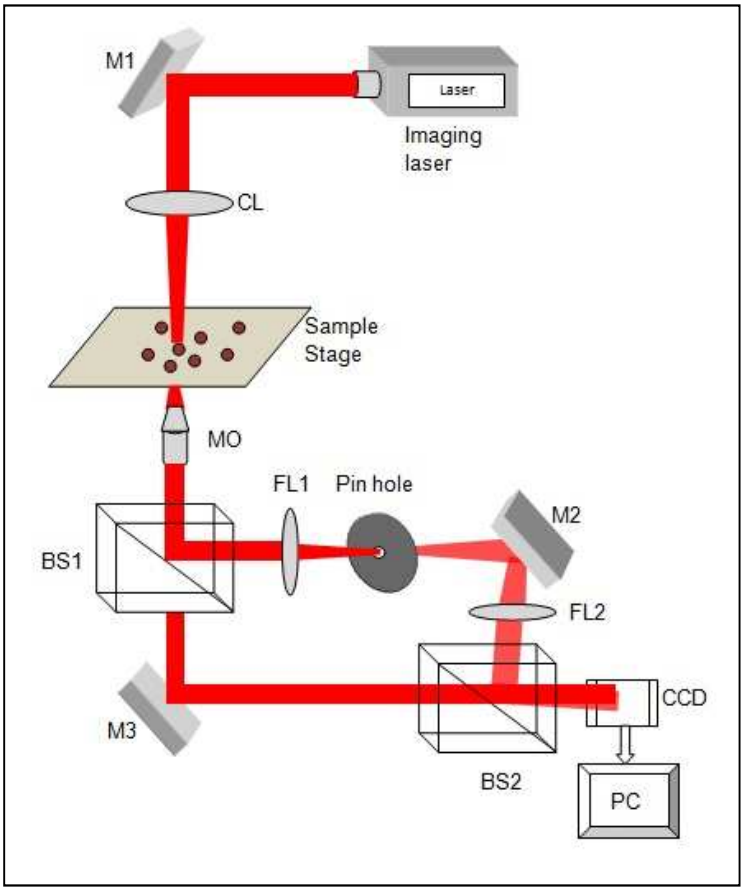


Figure 1-2: Schematic of Digital Holographic Microscopy set up. M1, M2, M3: Mirrors; CL: Condenser lens; MO: Microscopic Objective; BS1, BS2: Beam splitter; FL1, FL2: Focusing lens; CCD: Charge coupled device; PC: Computer.

The interference fringes follow the phase content of the sample and bend as per the wavefront information. Thus interference fringes bend more over the region of sample having high phase lagging contents. Acquired images are recorded by a program based on LABVIEW® where interference fringes are processed further to calculate phase image of sample. These phase images are then processed further in a program based on MATLAB® to get unwrapped pseudo colored 2D or 3D images.

## 1.6 Spatial Filtering

A lens has the capability of performing Fourier transform. The effect of a wave on a converging lens can be calculated by a transmission function shown in equation 1-1.

$$t(x,y)=e^{i\phi(x,y)} \tag{1-1}$$

A converging lens does not change amplitude of the wave if reflections from surfaces are ignored. It alters the phase of the traversing wave. A wave originating at point A $E_1(x_1,y_1)$ as shown in figure 1-3 propagating towards a converging lens can be approximated by Fresnel diffraction up to point B $E_2(x_2,y_2)$. Similar approach is used for propagation of wave from point C $E_3(x_3,y_3)$ to point D $E_4(x_4,y_4)$. Propagation of wave through a lens can be approximated by transformation of lens having focal length f. If the input wave is at focal plane of a lens and if output wave is seen at the back focal plane of a lens then it can be seen as two planes are related by a Fourier transform shown in equation 1-2 [23].

$$E_4(K_{x4},K_{y4})=\iint_{-\infty}^{+\infty} E_1(x_1,y_1)\,.e^{-i(K_{x4}x_1+K_{y4}y_1)}dx_1dy_1 \tag{1-2}$$

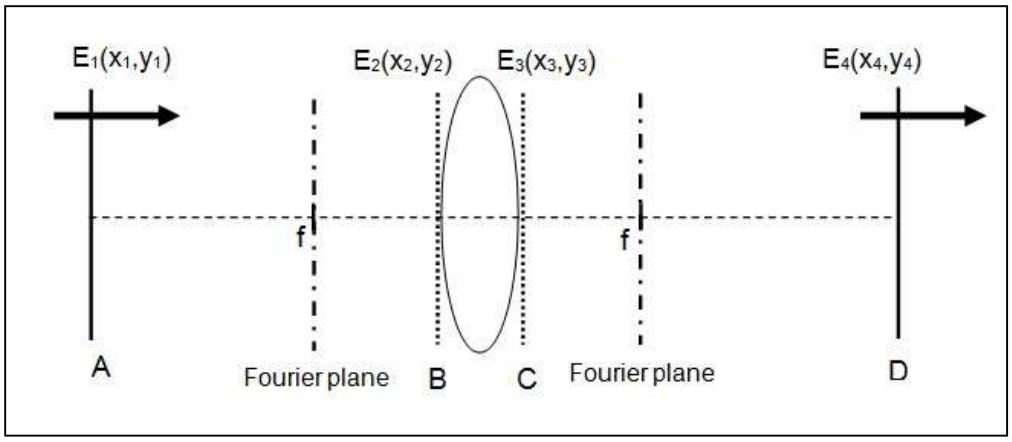


Figure 1-3: Lens as a Fourier transform. Propagation of wave from point A to Point D. Plane at f and back focal length of lens are Fourier transform of each other [23].

Thus by blocking out higher order spatial frequencies at the Fourier plane of a lens, a wavefront having no information about the phase of an object can be obtained. In this case, a pinhole of 25 μm does the trick. As shown in the figure 1-4, when a phase contained light wave comes at the focal plane of lens L1, its Fourier plane will show 0th order and $\pm$1st order. Selective filtering of lower order by a low pass filter (in this case a pin hole of 25μm size) removes all the higher orders and thus removing all the phase information contained by the incoming wave. The wave field is reconstructed by a lens L2 at its focal plane having Gaussian intensity profile with no information contained about the phase. This wave is called as reference wave (R) as it is more like imaging wave with no image information. This reference wave is allowed to interfere with object wave (O) in the beam combiner to form the interference pattern.

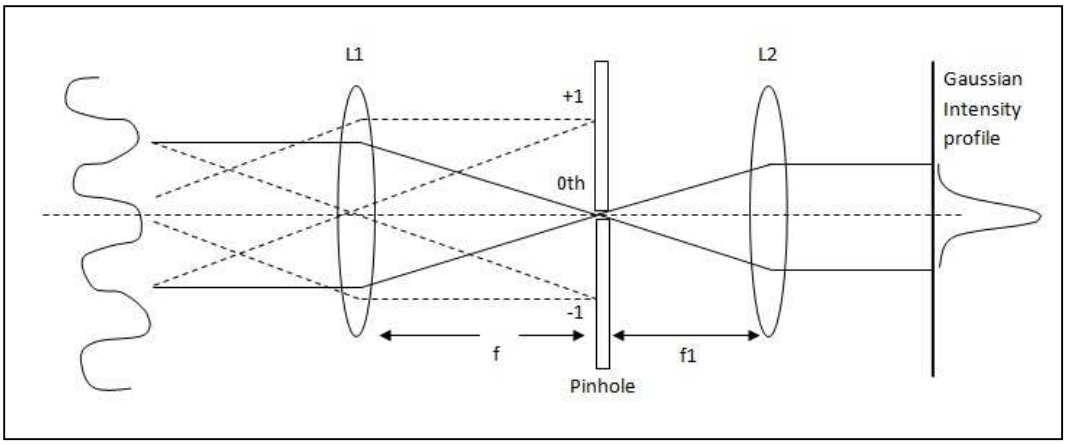


Figure 1-4: Spatial filtering of phase contained wave to get a collimated beam of Gaussian intensity profile with no phase information.

## 1.7 Off-Axis Method

"Fourier transform method of fringe pattern analysis for computer based topography and interferometry" was developed by M. Takeda in the year 1982, explains off axis geometry combined with FFT technique to process topographic images [24]. In this thesis, Digital holographic microscopy (DHM) using microscopic objective is described. Use of CCD in recording holograms increased resolution extremely [25][26]. In the off axis geometry, object wave (O) is allowed to mix with a reference wave (R) at an angle θ with respect to object wave (O). Since both the beams in this case are originated from a same source, the condition of coherent light for interference is fulfilled. Interference is energy redistribution process in which energy lost in destructive interference is compensated by gain in energy in constructive interference. If a wave is travelling at an angle θ with respect to another wave of same frequency, then phase difference at the point of intersection is given by

$$\Delta\varphi = \frac{2\pi d}{\lambda} = \frac{2\pi\,(x \sin\theta)}{\lambda} \qquad (1\text{-}3)$$

Where x is the overlapping beam width.

Constructive interference happens when waves are in phase while destructive interference takes place when waves are half a cycle out of phase. This constructive and destructive interference leads to formation of patterned interference fringes having fringe width or fringe spacing as shown in the following equation.

$$d_f = \frac{\lambda}{\sin\theta} \tag{1-4}$$

Thus, as in this case, wavelength is being kept constant; as θ increases, fringe width decreases.

These interference fringes follow the phase change observed by the light passing through a sample and hence bend according to the phase shifted. Studying these fringe patterns and by performing numerical calculations reveals the hidden information contained by the sample such as phase (refractive index and thickness).

## 1.8 Numerical Calculations

The hologram is produced by interference of object and reference beam at an angle θ. The holographic image is reconstructed using diffraction theory. Calculation of fringe pattern formed on CCD allows us direct access to amplitude and phase information of the sample. Numerical reconstruction in digital holographic microscopy can be done by approximating the propagation of optical field by Fresnel diffraction formula.

Thus the optical field at the CCD can be given by propagating the optical field at imaging plane $E_i(x,y)$ up to CCD plane $E_o(x,y)$ at a distance d from imaging plane by Fresnel diffraction formula [23].

$$E_o(x,y) = E_i(x,y) \otimes e^{\frac{ik_0}{2d}(x^2+y^2)} \tag{1-5}$$

As the object wave (O) is combined with reference wave (R), the total holographic field $E_t(x,y)$ as projected by CCD is given by

$$E_t(x,y) = E_o(x,y) + |E_r| e^{i(k_{rx}.x + k_{rz}.z)} \quad (1\text{-}6)$$

Where, krx = k.sinθ and krz = k.cosθ. θ is the off axis angle between object beam (O) and reference beam (R).

The intensity distribution of the hologram can be given by,

$$I_t(x,y) = |E_o(x,y)|^2 + |E_r|^2 + E_o(x,y).|E_r|.e^{-ik_{rx}.x} + E_o(x,y)^*.|E_r|.e^{ik_{rx}.x} \quad (1\text{-}7)$$

Taking the Fourier transform of equation 1-7 for digital reconstruction, we get

$$I_T(k_x,k_y) = FT[|E_o(x,y)|^2 + |E_r|^2] + E_o(k_x - k_{rx}, y).|E_r| + E_o(k_x + k_{rx}, y).|E_r| \quad (1\text{-}8)$$

The above equation can be compared with following equation.

$$I_T(k_x,k_y) = I_0(k_x,k_y) + I_{+1}(k_x,k_y) + I_{-1}(k_x,k_y) \quad (1\text{-}9)$$

The $I_0$ term does not contain any imaginary part and hence is a DC component i.e. 0th order of the image. $I_{+1}$ and $I_{-1}$ are $\pm$1st orders of the image. Selection of 1st order of the image yields information about phase contained in the sample. The term $E_o$ can be further expressed by Fresnel convolution if shifted back by $K_{rx}$. Taking Fourier transform of equation (1-5) and putting the term $E_i$ in the term I+1 we get,

$$I_1(k_x,k_y) = |E_r|.\ E_i(k_x,k_y)\ .\ e^{i\frac{d}{2k_0}(k_x{}^2+k_y{}^2)} \quad (1\text{-}10)$$

Thus, original field $E_i(x,y)$ can be obtained by taking inverse Fourier transform (IFT) of $E_i(k_x,k_y)$ hence switching it back to spatial domain. This component will give the phase information of the sample.

$$E_i(x,y) = IFT\left[ I_1(k_x,k_y)\ .\ e^{-i\frac{d}{2k_0}(k_x{}^2+k_y^2)} \right] \quad (1\text{-}11)$$

$E_i(x,y)$ is obtained after de-convolution which negates the effect of Fresnel propagation over the distance d.

The non ambiguous phase calculated from complex field varies within the interval of [-π, π]. Thus any other phase having the value over this range cannot be measured directly and needs further analysis. This effect caused by the phase values outside the range of [-π, π] is called as wrapping effect. These phase values can essentially be calculated by a mathematical technique called as phase unwrapping.

The unwrapping program used here is based on Goldstein's algorithm [27] which looks for 2π jumps in the signal and adds the 2π value back to the signal. It calculates the slope of the line and divides the line with the slope to make a flat line. Any other slope which is greater than the slope of line calculated is measured as phase of the object. Figure 1-5 illustrates the operation.

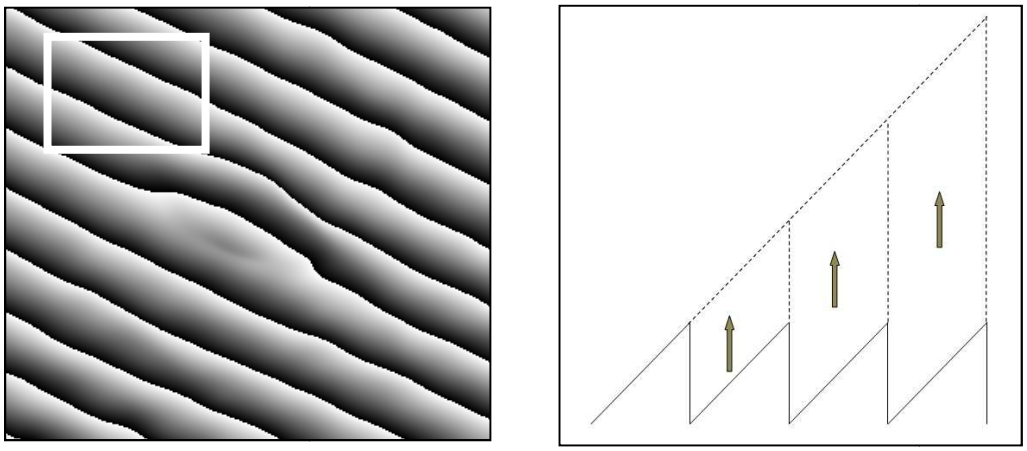

(a) (b)

Figure 1-5: Unwrapping method (a) Reconstructed fringes showing wrapping effect for a cell (b) 2π jumps for fringes shown in the box in (a) and addition of the values back to the signal.

The phase information obtained from unwrapping algorithm can be used to calculate other quantitative unknowns such as refractive index, thickness using the following equation.

$$\varphi = \frac{2\pi}{\lambda}(n_1 - n_0).d \qquad (1\text{-}12)$$

Where, φ is phase, $n_1$ is refractive index of sample, $n_2$ is refractive index of surrounding medium, d is physical thickness of the sample and λ is wavelength used.

## 1.9 Limitations of Digital Holographic Microscopy

DHM works on the principle of measuring phase of the sample under observation. Phase of the sample calculated with DHM is relative to the surrounding medium of sample. Cells shift optical phase of light passing through it. The amount of phase shift depends on the integral refractive index of sample and physical thickness of the sample as well as refractive index of surrounding medium and wavelength of light. DHM will detect the sample when there is difference in refractive index of sample and its surroundings. The problem lies in detecting the sample when refractive index of sample is very close to that of surrounding medium. In this case, the sample might get lost in background noise. However, cell's or any of its part's refractive index may be increased by addition of contrast agents. Another problem faced by DHM is background noise. As DHM imaging is done by a coherent light source, it is very sensitive to light refraction, reflection and change in polarization [28]. Large amounts of efforts have been dedicated towards reducing the background noise in the system. Especially, the speckle noise (due to coherent light) can be reduced by use of rotating diffuser. Also, use of low and non-coherent (white light) light is finding more use in DHM for reducing coherent noise.

# Chapter 2

# NIR QPM Under Silicon

## 2.1 Introduction

Recent advances in biological and chemical analysis have led to the development of miniaturized, lab-on-a-chip technologies that can be used in a diverse array of applications which includes cell studies [29], [30] immunoassays and DNA analysis [31]. These devices can be used in combination with electrostatic, magnetic and micro-mechanical manipulation techniques to achieve a variety of objectives such as improvement of speed of analysis, use of relatively smaller fluid volumes and shorter reaction times of biological samples. Silicon has been primarily used for fabrication of miniaturized lab-on-a-chip devices; moreover many MEMS devices are also silicon based and thus it has also been used in the development of implantable devices [32]. The thing that makes silicon so desirable for manufacturing purposes is that it is abundant and it has an impurity. This makes the manufacturer possible to control the conductivity of the sample by varying the impurities. Silicon wafers can also be etched to change the conductivity along the well defined channels in the wafer [33]

There is a clear need of enhanced microscopic technique to image manipulation processes through the opaque silicon lab-on-a-chip devices. Because cells primarily affect the optical phase of light passing through them, visualization of the phase modulation that occurs when light traverses these specimens could provide additional information. Near infrared microscopy has gained increased interest in the scientific research in cellular microscopic study. Some of the silent features of near infrared microscopy include very low auto-fluorescence for exceptionally low backgrounds. Lower energy NIR wavelengths have high penetration ability and cause less sample damage as compared to visible wavelengths. Near infrared quantitative phase microscopy (NIR-

QPM) is an innovative technique to visualize and characterize microscopic objects through silicon.

Figure 2-1 shows different techniques to manipulate cells on silicon substrate. Cells can be stimulated electrically or mechanically. Readings can be obtained either electrical or mechanical or both depending on the aim. Sensed signal is sent to micro device which characterizes the signal.

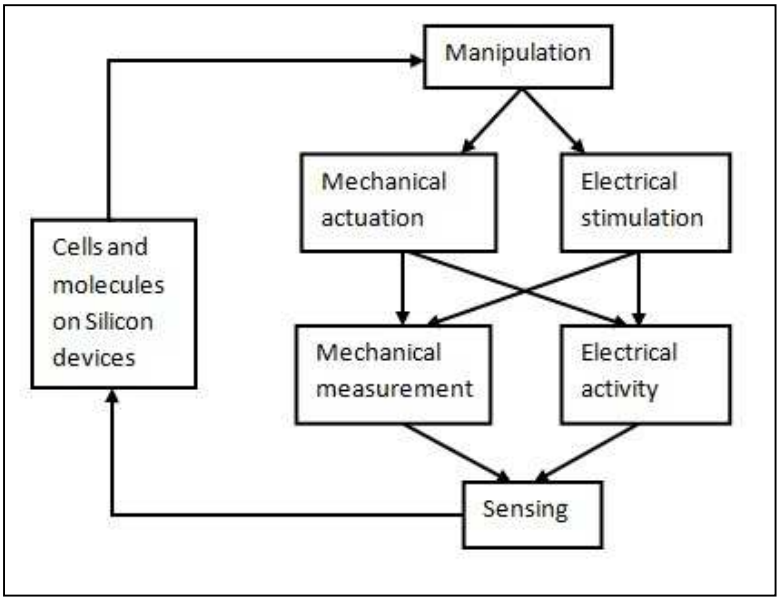


Figure 2-1: Different manipulations of cells on silicon based devices.

## 2.2 Experimental Setup

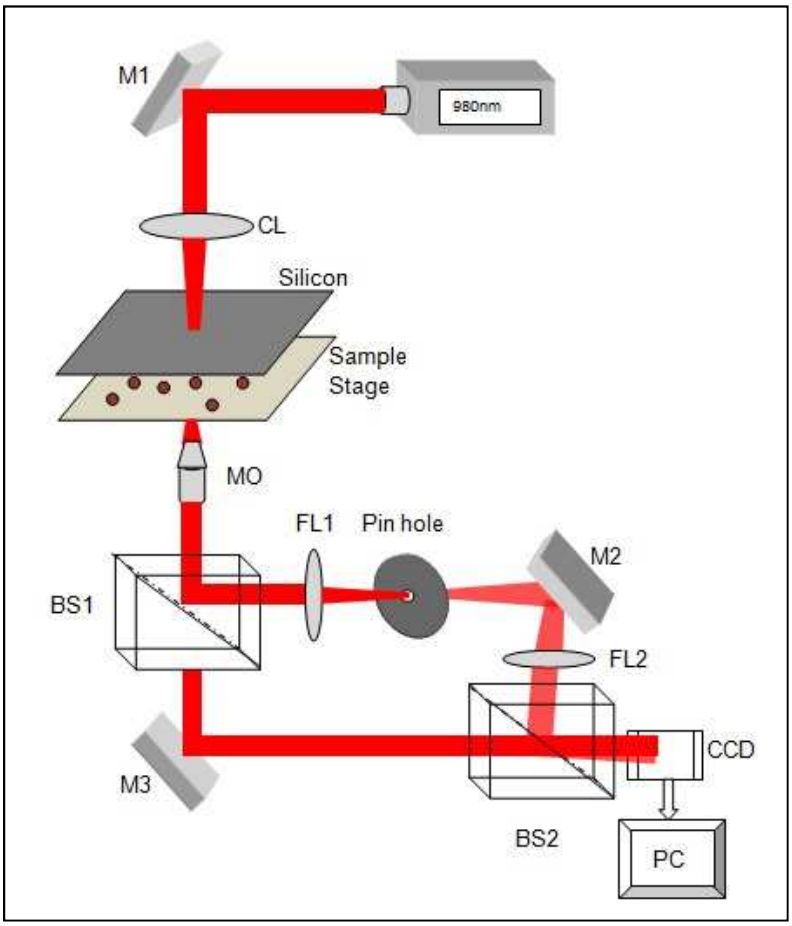


Figure 2-2: Schematic diagram of near infrared QPM setup for characterizing samples through silicon. HL: Holographic laser for DHM; CL: Condenser lens; MO: Microscopic objective; BS1&BS2: Beam splitters; M1&M2: Mirrors; FL: Focusing lens; PH: Pin hole; CCD: Charged couple device; PC: Computer.

The NIR-QPM setup as shown in Figure 2-2 consists of a tunable Ti: Sapphire laser source (690 to 1040 nm). However, for NIR-QPM, we used 960 nm to 1040 nm range of the available spectrum. Condenser lens (CL) concentrate the light on the sample placed below the silicon wafer. Silicon wafer of 100 µm thickness is used. A xyz-

translational stage helps to position the sample. Light transmitted through the silicon wafer and sample is collected by a microscopic objective (MO) and is split into two beams by a beam splitter (BS1). One of the beams is made to serve as reference beam by spatially filtering it using a pin hole (25µm). Light coming out of the spatially-filtered beam does not contain any phase information of the specimen and thus act as reference beam. The other beam which is not spatially-filtered (Object beam) is permitted to mix with reference beam in another beam splitter (BS2) at an angle in off-axis geometry. Combining reference beam and object beam form an interference pattern of dark and white bands. The angle between the reference beam and object beam can be changed by changing the mirror positions (M1 & M2). The interference pattern is recorded by a CCD camera and images are acquired at 14 frames per second. The acquired images are processed and the holographic diffraction is calculated by programs based on LabVIEW® and MatLab®.

## 2.3 Performance characterization

Since silicon is opaque in visible spectrum, and since we are using near infrared (NIR) wavelengths to observe and image specimen under silicon; it is necessary to study transmission of silicon in the NIR region. To determine the performance of silicon in NIR region, its transmission in a range of wavelengths is measured. To analyze the image quality obtained using Si-based CCD, image contrast is measured along the same range of wavelengths. Furthermore Noise in the system is calculated for a selected wavelength to determine the resolution of the system.

### *2.3.1 Transmission through Silicon*

Transmission of laser through silicon is measured to understand capability of silicon to transmit the wavelengths in NIR region through. This is done by keeping the incident laser (Ti: Sapphire) power constant at 14.7 mW and measuring the laser power after it

has passed through 100 μm thick silicon wafer and collection optics ( microscopic objective). The transmitted laser power is measured by a power meter (PM100D, Thorlabs Inc.) across a set of wavelengths ranging from 960 nm to 1040 nm.

Table 2-1: Transmission through silicon.

| Laser Wavelength (nm) | Transmission (mW) | Transmission (%) |
|---|---|---|
| 960 | 0.735 | 5 |
| 980 | 0.882 | 6 |
| 1000 | 1.764 | 12 |
| 1020 | 2.205 | 15 |
| 1040 | 2.499 | 17 |

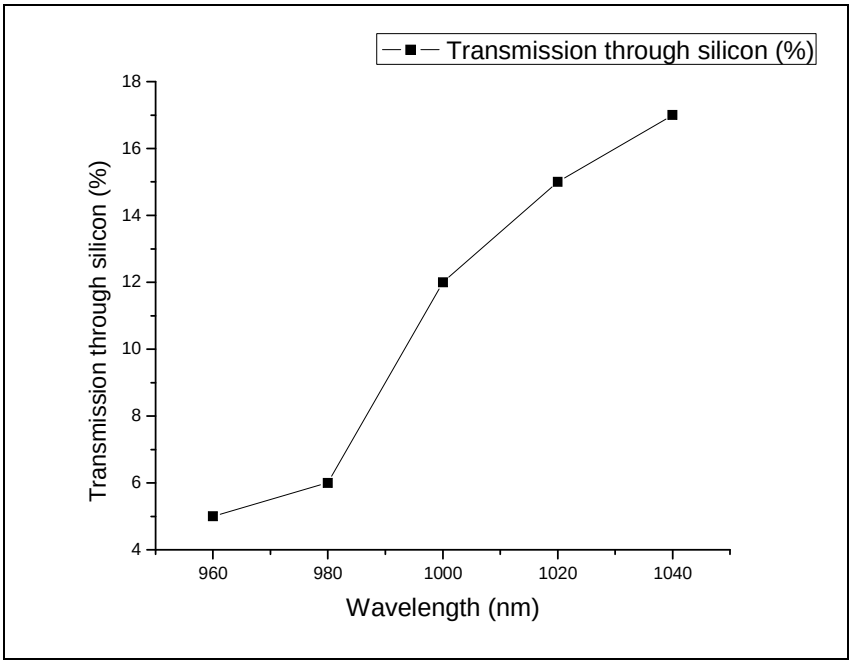


Figure 2-3: The transmission spectrum of Silicon in NIR wavelengths.

Table 2-1 above shows the original values for transmission as well as percentage values of transmission of laser through the silicon for incident power of 14.7mW being

kept constant for all the wavelengths. Figure 2-3 shows the graph of percentage transmission across wavelengths. From the graph, we can see that transmission of laser through silicon increases as we increase the wavelength in near infra-red.

*2.3.2 Fringe contrast dependence*

CCD chip is made of silicon and since silicon shows increased transmittance in NIR region, it is therefore necessary to understand interference fringe contrast in NIR wavelengths. Fringe contrast is particularly important because clarity and stability of $\pm 1^{st}$ order which is obtained after taking FFT of the bright field image; largely depends on the contrast of interference fringes.

Fringe contrast is calculated by the formula shown in equation 2-1 as both white and dark bands are equivalent and take up similar fractions of the area.

$$C = \frac{I_{max} - I_{min}}{I_{max} + I_{min}} \tag{2-1}$$

Interference fringes are recorded for various wavelengths in near infrared region, to calculate fringe contrast. Figure 2-4 shows recorded interference fringe images for 960nm, 980nm, 1000nm, 1020nm and 1040nm. The values for contrast along with its standard deviation for selected wavelengths are shown in the Table 2-2 above. Graph in the Figure 2-5 shows decreased fringe contrast along the wavelengths. This shows that silicon chip CCD has higher sensitivity in lower NIR wavelengths.

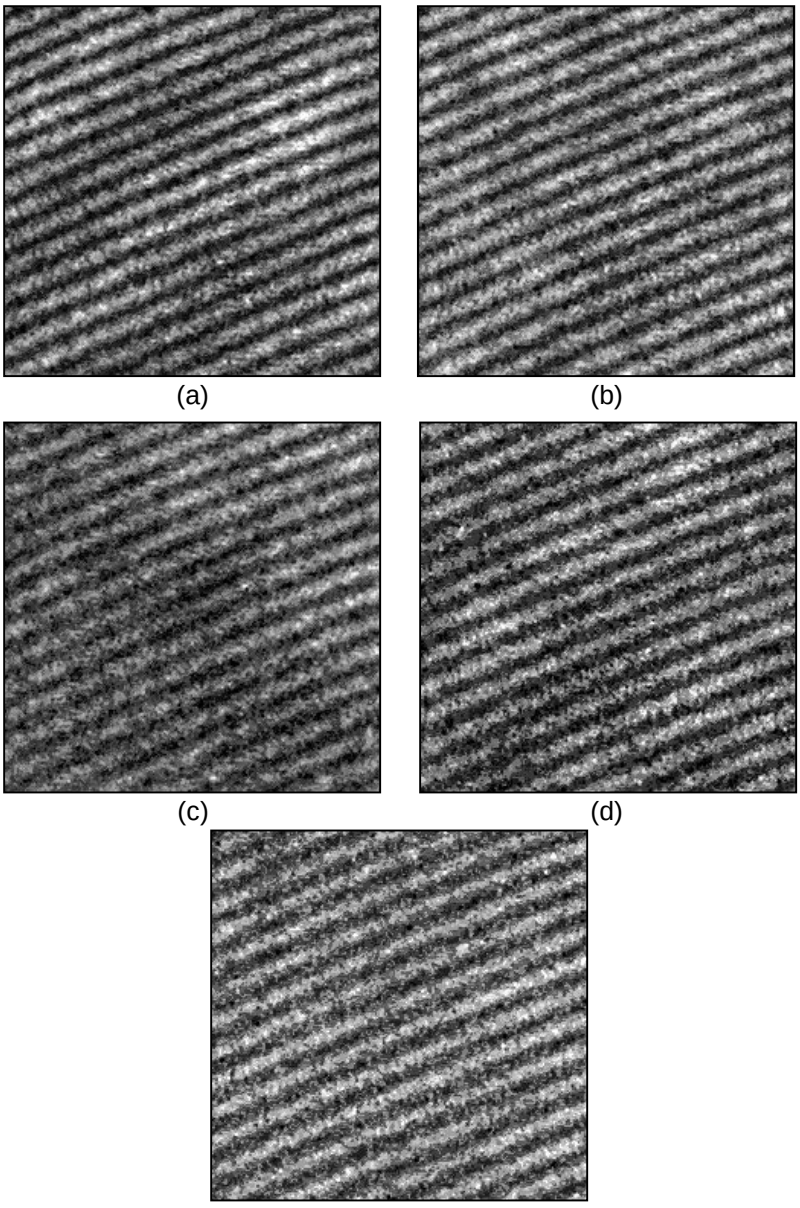


Figure 2-4: Interference fringes at (a) 960nm (b) 980nm (c) 1000nm (d) 1020nm and (e) 1040nm.

Table 2-2 Fringe contrast calculated mean and standard deviation

| Wavelength | Mean | Standard deviation |
|---|---|---|
| 960 | 0.44 | 0.024 |
| 980 | 0.36 | 0.012 |
| 1000 | 0.25 | 0.021 |
| 1020 | 0.22 | 0.022 |
| 1040 | 0.22 | 0.021 |

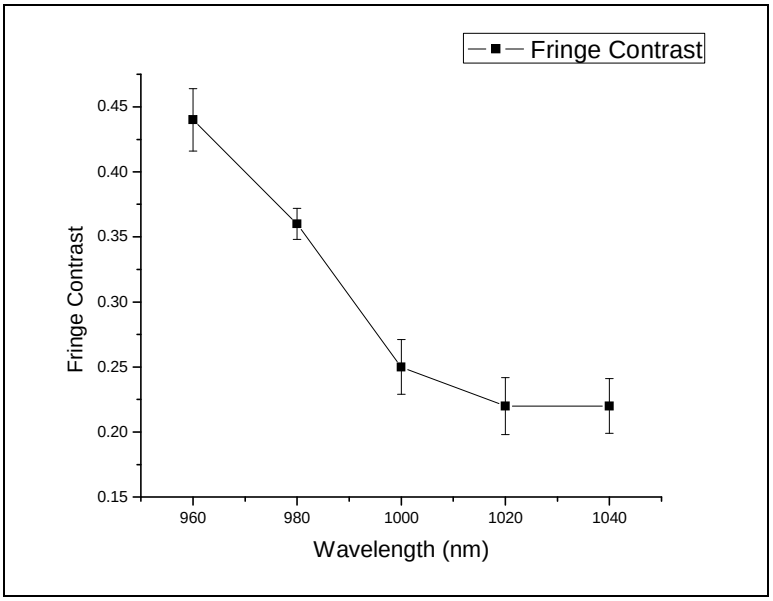


Figure 2-5: Fringe contrast graph against wavelength. Graph shows decrease in fringe contrast as wavelength is increased.

Taking into consideration the better transmission of higher wavelengths through silicon and CCD camera's higher sensitivity at lower NIR wavelength, a wavelength of 980 nm is selected for imaging through silicon.

*2.3.3 Noise calculation*

It is important to determine noise inherited in the system to test the system's resolution and sensitivity. Noise is analyzed by calculating variation in phase over a region over time. To compute system's resolution, optical path length variation over time for every recorded image is calculated using the formula:

$$\varphi = \left(\frac{2\pi}{\lambda}\right).P \qquad (2\text{-}2)$$

Where, □ = phase, λ = wavelength and P is optical path length, which is defined as:

$$P = n \,.\, d \qquad (2\text{-}3)$$

Where n = refractive index of the material and d = thickness of the material

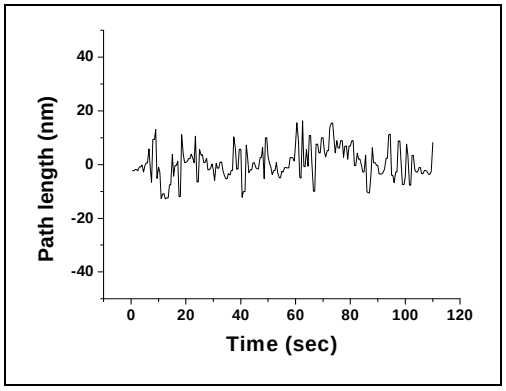


Figure 2-6: Path length variation over time.

Polystyrene particles of 6 μm in diameter and refractive index of 1.59 are used to calculate phase variation over time. By using the formula (2-2), path length variation is calculated. As refractive index and thickness of the sample will remain permanent, path length will only change if phase changes. The average path length variation is 6nm. Figure 2-6 shows optical path length variation in nm over time.

## 2.4 Validation of setup

In order to validate the new special filtering based Digital Holographic Microscopy setup, phase measurements were carried out on polystyrene particles of known size of 6µm having refractive index ($n_1$) of 1.57. Oil is used as a reference refractive index medium i.e. polystyrene particles are immersed in oil ($n_2$=1.50). A Ti: Sapphire laser of 980nm wavelength is incident on polystyrene particles through a silicon wafer. Phase of the polystyrene particle is calculated by the information obtained from interference fringes formed on CCD.

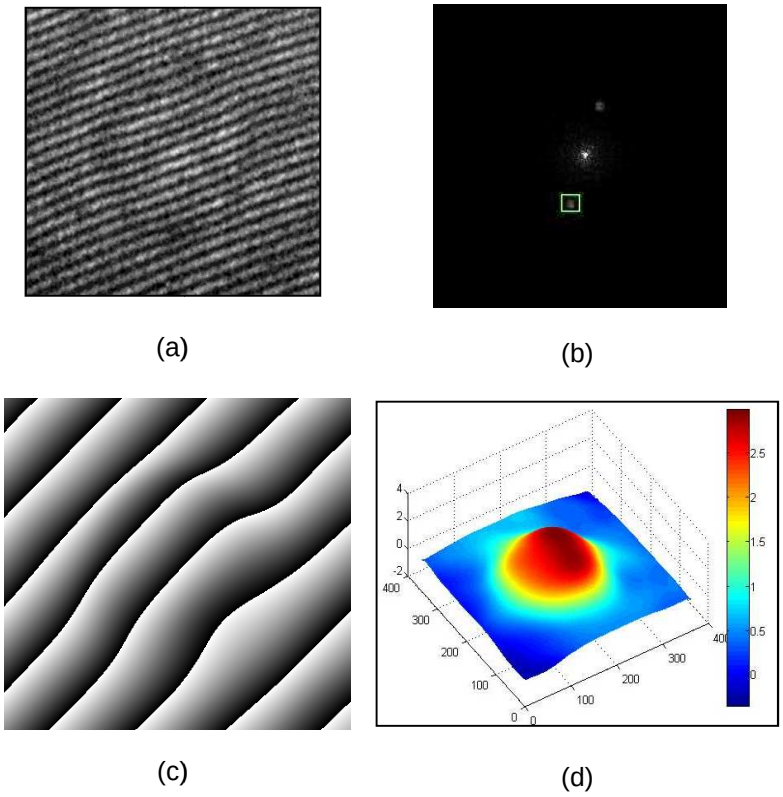


Figure 2-7: DHM of Polystyrene particle (a) NIR bright image of 6µm polystyrene particle in immersion oil. (b) FFT of bright field image and selection of 1st order (c) Reconstructed fringes from selection (d) Reconstructed 3D image showing phase value for 6 micron Polystyrene particle in immersion oil ($n_2$=1.51).

Figure 2-7 shows bright field image of a polystyrene particles. Interference fringes in the figure can be seen bending over the particle because of optical phase shift. FFT of the bright field image is shown in Figure 2-7(b). 1st order is selected as $\pm$1st order contains all the information about phase. Figure 2-7(c) shows the reconstructed fringes after selecting 1st order in FFT. These reconstructed fringes are then processed in Matlab® to get the unwrapped image as shown in Figure 2-7(d). The unwrapped image shows the phase value of 2.69. If put in the equation (2-4) shown below, value of n1 (refractive index of polystyrene particle) comes to be 1.569.

$$n_1 = \left( \frac{\varphi \,.\, \lambda}{2\pi \,.\, d} \right) + n_2 \qquad (2\text{-}4)$$

## 2.5 Investigation of biological structures

NIR QPM is a valuable experimental tool for structural and functional biological specimen investigations. To examine biological structures, human RBCs (red blood cells) are imaged using NIR QPM under silicon environment.

Fresh human RBC cells ($n_1$=1.39) are kept in isotonic fluid so that shape of RBCs remain intact. These RBCs are imaged through silicon for thickness measurement. Bright field image of RBCs imaged by using a microscopic objective of N.A. 0.65 are shown in Figure 2-8(a). Notice that one of the three RBCs is tilted at an angle. Figure 2-8(b) shows the reconstructed fringes after selecting $1^{st}$ order of FFT of interference pattern. A 3D representation of the phase of three RBCs is reconstructed as shown in Figure 2-8(c). The ring like structure of the RBC can be clearly seen in top view. As middle RBC is tilted, it has higher phase as compared to rest of the two RBCs. The tilted RBC creates a larger phase shift of light passing through it and thus is showing higher phase value.

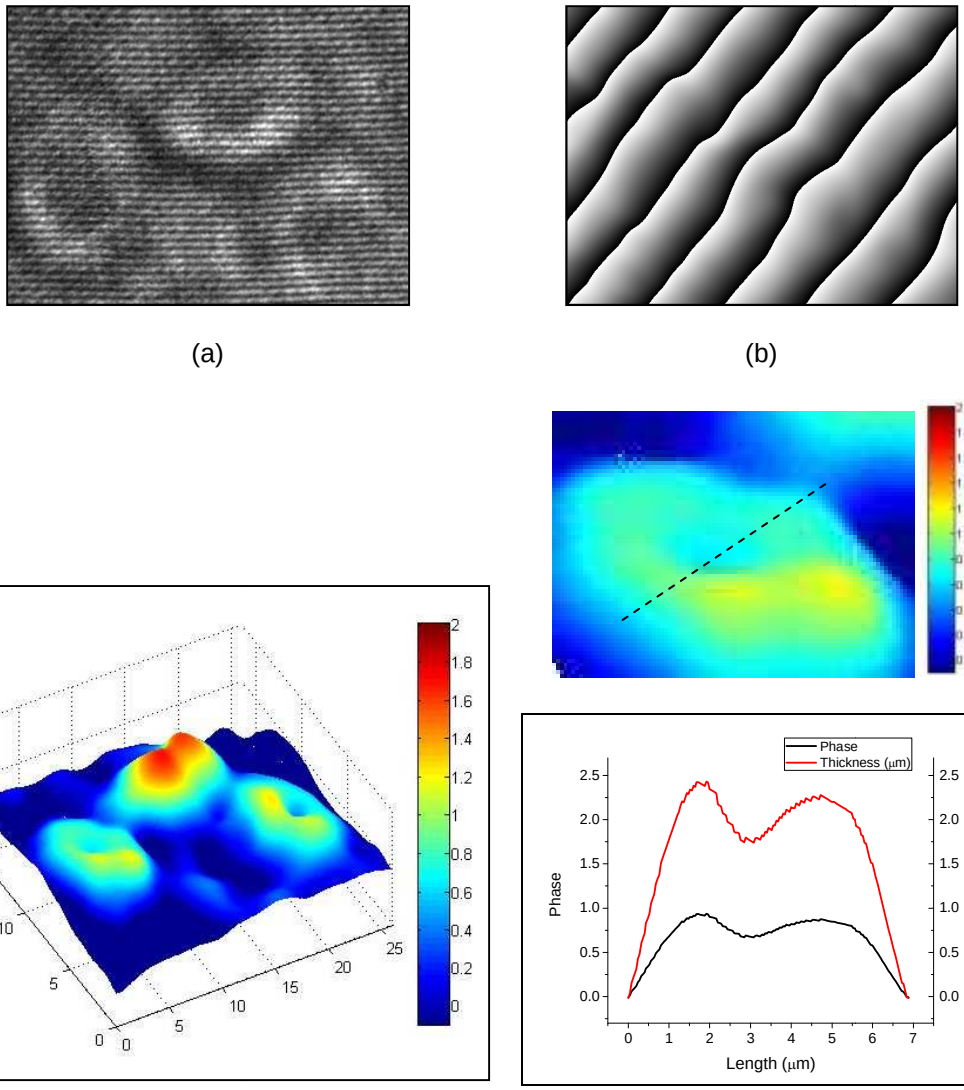


Figure 2-8: Characterization of RBCs under silicon. (a) Bright field image of RBCs (b) Reconstructed fringes (c) Reconstructed 3D phase map (d) selection of a RBC and a line along which phase values are taken. Graph showing phase profile and thickness profile of single RBC overlaid.

One of the RBCs is selected and measured for the phase values along the line shown in Figure 2-8(d). Graph in the Figure 2-8(d) shows phase values of the selected RBC plotted against position in µm. Thickness of RBC is calculated from phase values taken along the line using following equation.

$$d = \left( \frac{\varphi \cdot \lambda}{2\pi (n_1 - n_2)} \right) \tag{2-5}$$

## 2.6 Stimulation under silicon

### *2.6.1 Methods*

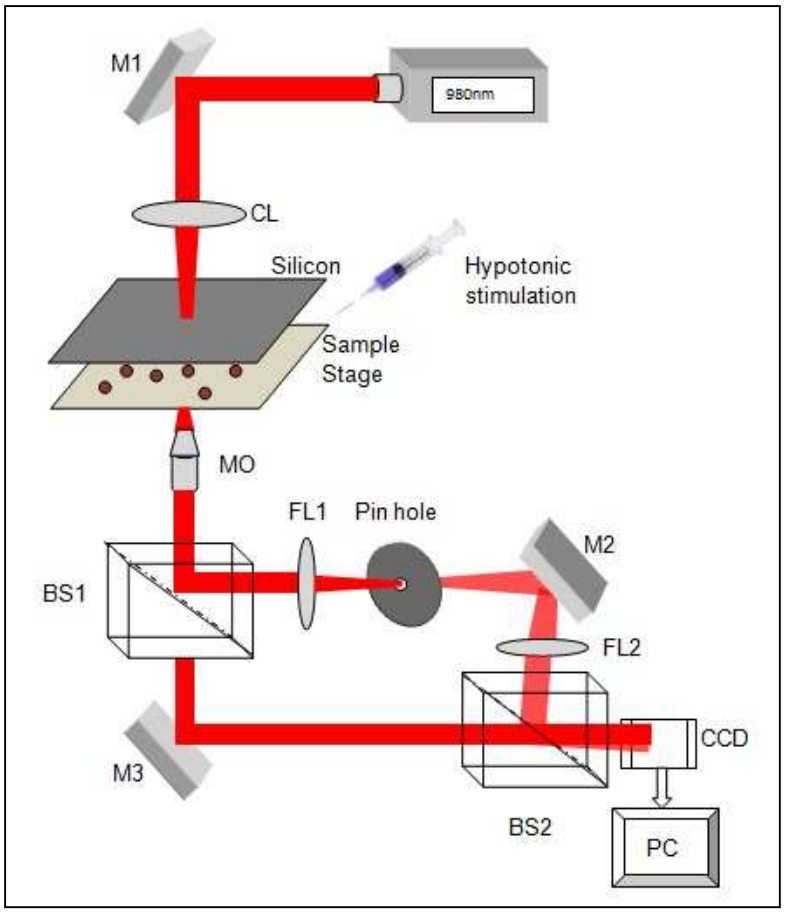


Figure 2-9: NIR QPM setup for hypotonic stimulation under silicon.

Silicon is used for many different applications in cell studies. The NIR QPM setup is effectively used to image the cells and particles through the silicon. It is necessary to investigate cellular activity under the silicon. To study the cellular kinetics, cells are stimulated and imaged through silicon using the new NIR QPM setup as shown in Figure 2-9.

Intracellular components contribute largely towards determining the mean integral refractive index of the cell. Thus cells are imaged at a wavelength of 980 nm by a Ti: Sapphire laser beam for phase measurements. Any physiological change in the cell will reflect directly on the mean refractive index and/ or physical thickness of the cell, thus on the phase measurements of the cell.

Cells examined for hypotonic stimulation were HEK (Human Embryonic Kidney-293) cells. These cells are first measured for phase values in normal isotonic solution (300 mOsm/Kg). A hypotonic shock is then given to the cells by changing the osmolarity of the extracellular solution. For inducing hypotonic shock, predetermined amount of distilled water or a salt solution having osmolarity less than 300 mOsm/Kg is added in the solution containing cells. Physiological changes in the cells are then recorded by the NIR QPM setup by calculating phase of the cells. All the measurements are performed at room temperature.

## 2.7 Results and Discussion

### *2.7.1 Stimulation by hypotonic NaCl solution*

#### 2.7.1.1 Preparation of Hypotonic NaCl solution

The isotonic solution contains 0.9% of NaCl concentration. A total concentration below 0.9% will make the solution hypotonic for cells. 3ml of distilled water is added to 1 ml of isotonic solution, so as to make the solution hypotonic. Thus, now the 4 ml solution

has NaCl concentration of 0.225%. The total osmolarity of the solution is therefore 75 mOsm/Kg.

To see the effect of hypotonic stimulation on living cells under silicon wafer, HEK cells are stimulated by hypotonic stimulation and are imaged using a Ti: Sapphire laser at 980 nm under a 100X objective having N.A. of 1.25. All the measurements are performed at room temperature and off-axis holograms of the cells are recorded before as well as after the hypotonic shock. From the DHM phase images, kinetics of the phase of the cell is obtained. Figure 2-10 (a) shows the bright field image of the cell. Reconstructed fringes are shown in Figure 2-10 (b). A 3D phase plot showing the phase of cell in isotonic solution is shown in Figure 2-10 (c). To induce cell swelling, isotonic cell culture medium (300 mOsm/Kg) is made hypotonic by addition of hypotonic solution having the osmolarity of 75 mOsm/Kg to a final osmolarity of 187 mOsm/Kg. To see the effect of hypotonic stimulation on the cells, a 600µl of hypotonic solution is added into the dish containing 1ml of media to change the osmolarity of the solution to 215 mOsm/Kg. This change in osmolarity induces fluid intake inside the cell and causing total increase in cell thickness. Due to increased thickness of the cell, phase value is expected to increase; as optical phase shift will be more for increased thickness. To the contrary, phase of the cells are observed to decrease in value.

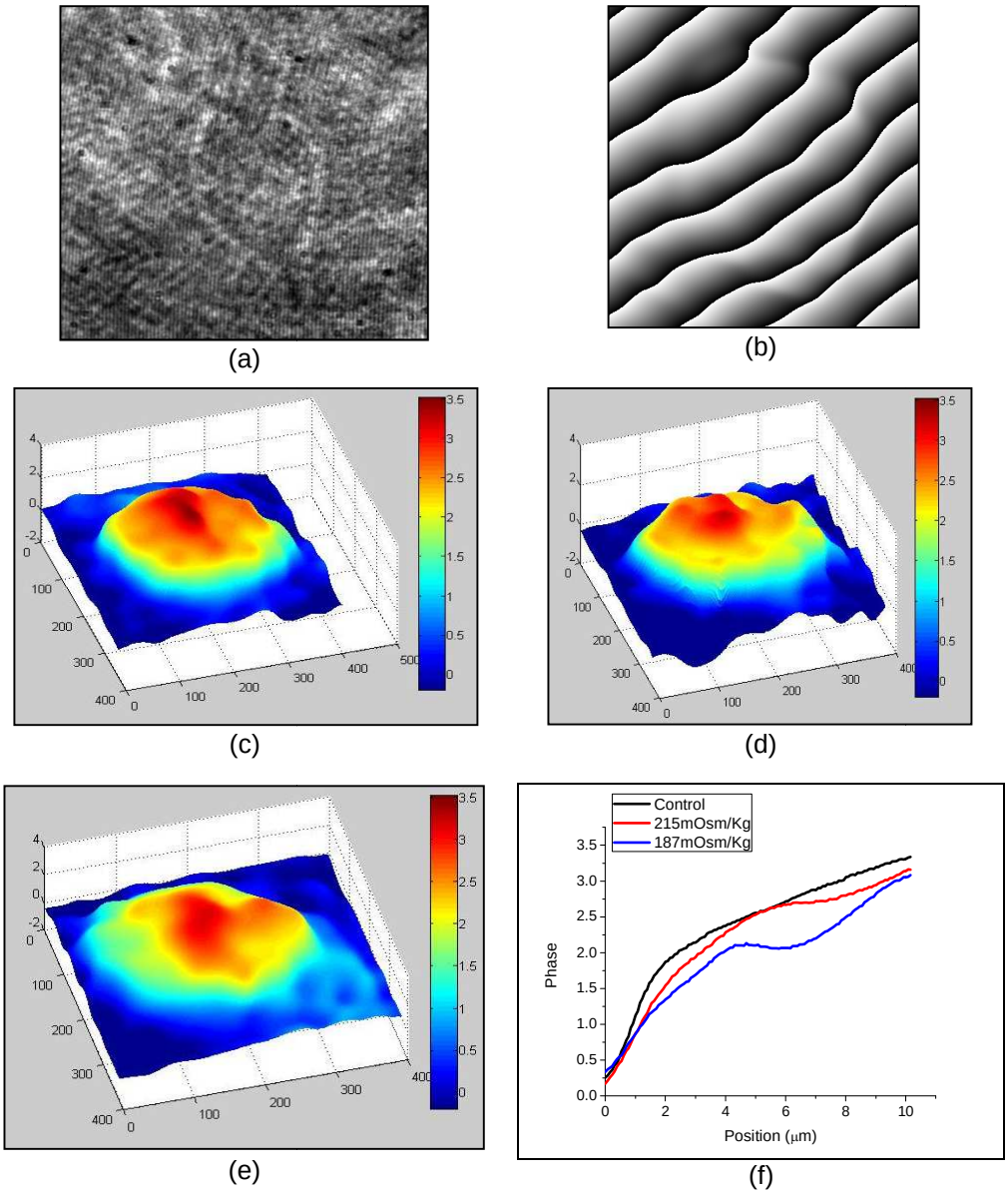


Figure 2-10: Characterization of hypotonic stimulation through silicon for one cell (a) NIR image of a HEK cell in isotonic solution as on CCD using 100X objective. (b) Reconstructed fringes of the image. (c) Unwrapped 3D phase image of HEK in isotonic solution. (d) 3D phase image in 215 mOsm/Kg hypotonic solution. (e) 3D phase image in 187 mOsm/Kg hypotonic solution. (f) Graph showing phase profiles of HEK cell from nucleus to its membrane over repeated hypotonic shocks.

Unwrapped 2D images when compared for phase values before and after hypotonic shock, shows decreased phase after the shock as shown in figure 2-10 (c) and 2-10 (d). This decrease in phase is because of water influx inside the cell; which causes dilution of some proteins inside the cell. As intracellular protein concentration largely determines the mean integral refractive index, dilution of the same results in the decreased phase values. The cell is objected to further hypotonic shock of 400 µl so that total hypotonic shock becomes 1 ml, the osmolarity of the solution decreases down to 187mOsm/Kg. This decreased tonicity causes more influx of fluid inside the cell diluting more proteins; and thus resulting in further decreased phase as shown in Figure 2-10 (e). To characterize change in phase values, a phase profile over a line along the cell from its nucleus to the membrane is shown in the Figure 2-10 (f). The figure shows decreased phase values for every other hypotonic stimulation.

*2.7.2 Stimulation by distilled water*

To see the effect of hypotonic stimulation on living cells cumulatively under silicon wafer, HEK cells are imaged using a 40X objective with N.A. of 0.65 for hypotonic stimulation. Digital off axis holograms of the cells are recorded before as well as after hypotonic shock.


(a) (b)

Figure 2-11: Bright field image of HEK cells (a) under 40X (b) Zoomed image showing fringes.

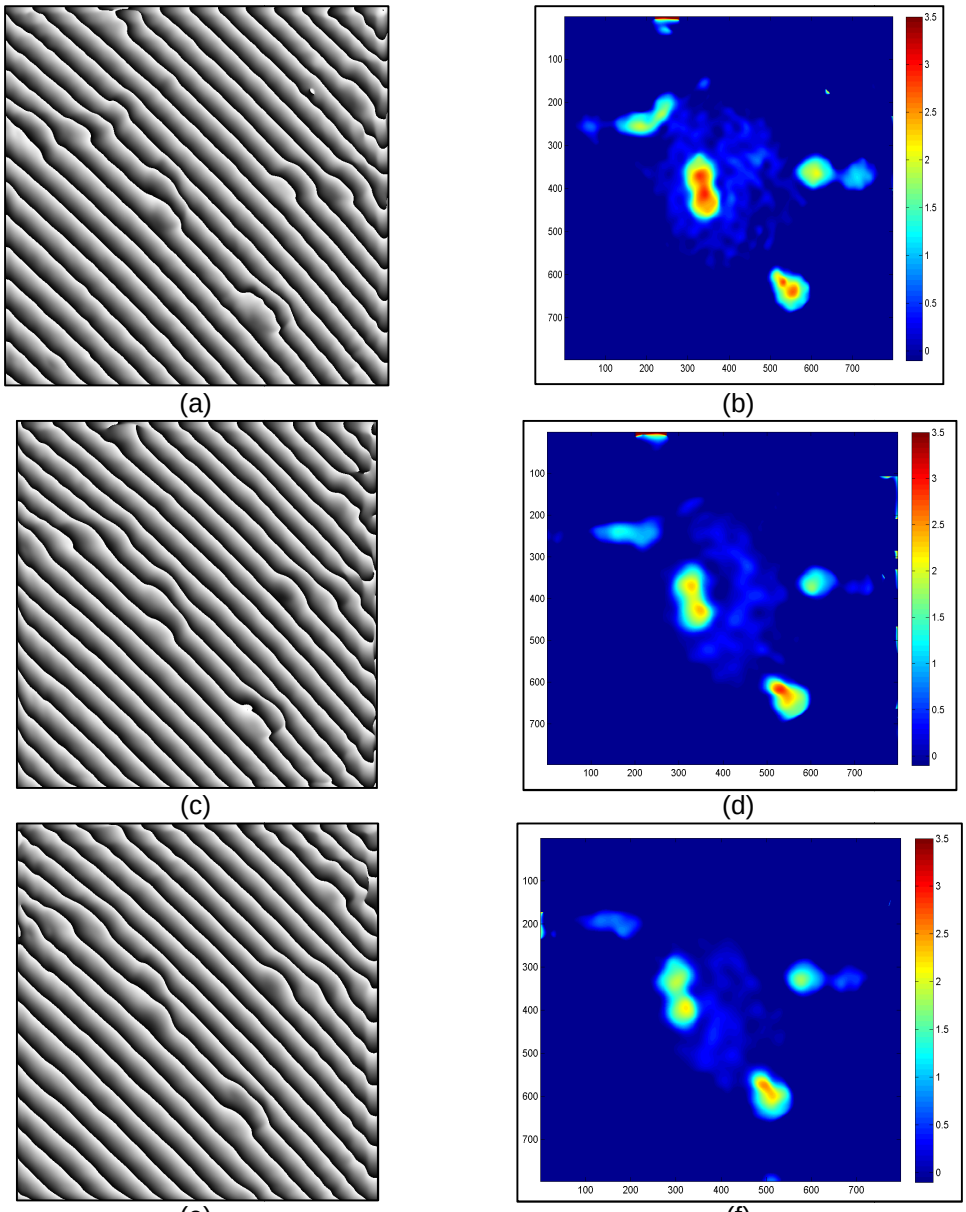


Figure 2-12: DHM of 6 HEK cells under silicon for hypotonic stimulation (a),(c),(e) Reconstructed fringes of HEK cells in Isotonic (a) and (c),(e) hypotonic solution (b),(d),(f) Unwrapped 2D image showing phase values for HEK cells in Isotonic (b) and hypotonic solution (d),(f).

Figure 2-12 shows the effect of hypotonic stimulation on six HEK cells. Bright field fringes are shown in Figure 2-11 (b) while reconstructed fringes are shown in Figure 2-12 (a). 2D unwrapped image showing the phase of the cells is shown in figure 2-12 (b). Cells are stimulated by making the extracellular solution hypotonic to the cells. 500 µl of distilled water is added into the extracellular solution to induce first hypotonic shock. This addition of distilled water into 2 ml of isotonic cell culture media reduces the osmolarity of the medium from 300 mOsm/Kg down to 240 mOsm/Kg.

Hypotonic stimulation will bring about a change in concentration of solutes in the extracellular medium. This persuades intake of fluid inside the cell and results in total increased thickness of the cell because of cell swelling. All the phase images are recorded after 2 minutes of hypotonic shock without changing any parameter. Comparison of unwrapped 2D images before and after hypotonic shock show decreased phase value after hypotonic stimulation. This decrease in the phase is because of water influx. This influx results dilution of intracellular protein concentration and is consistent with a water influx. Another hypotonic shock of 500 µl of distilled water on top of this shock was administered to see the effect on the cell phase values. This second shock makes the extracellular medium more hypotonic to the cells changing the total osmolarity of the medium down to 200 mOsm/Kg. Captured images show further decrease in the phase value of cells.

Graph in Figure 2-12 shows the decreased phase values for the osmolarity of 200 mOsm/Kg. This shows the dilution of protein concentration is consistent with water influx. Graph in the Figure 2-12 shows phase variation of selected portions of cells over time. Graph shows mean phase values of the selected region over cells. A region over cell is selected by selecting a window in Matlab® program. Mean phase value of the

selected portion is given by the program and is plotted over time. This is repeated for 6 different regions.

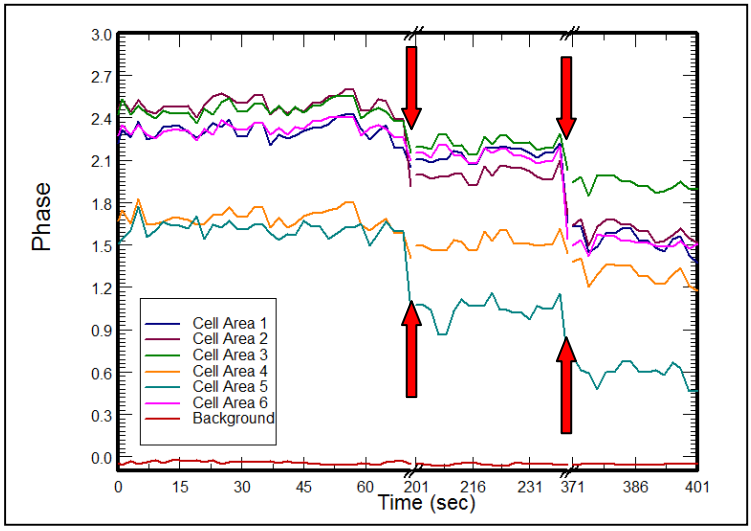


Figure 2-13: Graph showing phase variation of HEK cells over repeated hypotonic shocks shown by arrows.

The mean phase value for different areas of cells before stimulation is 2.137. After first hypotonic shock, it decreases to 1.827 and for second hypotonic shock; it reduces further down to 1.397.

# Chapter 3

# DHM Imaging Of Optically Stretched Cells

## 3.1 Introduction

Cells are elastic and can be deformed by subjecting them to a mechanical force arising from their external environment [34],[35]. Cells are subjected to biochemical and biomechanical environment throughout their life time. Biomechanical forces play an important role in maintaining a cell's normal development as well as form and functions. The effect of external mechanical forces on cells is very important to understand because these forces have been shown to regulate many types of cell processes which include proliferation, differentiation, migration and cell cycle progression [36]-[38]. Diseased cells vary in their physiological and chemical properties from normal cells; changing their elasticity and refractive index and thus affecting viscoelastic properties [39]-[43]. Researchers have been studying biophysical property i.e. elasticity of cells by atomic force microscopy [44],[45] or by micropipette aspiration [46] or by optically stretching cells using optical tweezers [34],[35]. Since progression of the disease pathophysiology is reflected in the biophysical properties of the cells, it is possible to identify the changes in the cells optically by measurement of refractive index and elasticity.

Recent experiments have shown that normal cells and malignantly transformed fibroblast cells deform to different extent when stretched by optical tweezers. Nevertheless these experiments have been done by attaching high refractive index beads to the cell wall. High refractive index beads can be trapped by forming an optical trap and by means of the trap a cell can be stretched and measured for its elasticity. Though this enables measurement of possible effects of chemical factors, disease states etc [47], it has very low throughput and cumbersome to perform.

HOX B9 is a protein which is encoded by HOXB9 gene in humans. These genes are widely recognized as transcription factors which bind to its target gene promoters. Over expression of transcription factors has been known as a reason of assisting tumorigenesis [50]. Over-expression of HOX B9 protein in normal HEK cells compels these cells to form colonies indicating over expression of HOX-B9 can be a potential contributor towards tumorigenesis [51]. Transformation of healthy cells into malignant cells has been reported to cause change in cell's viscoelastic properties [43].

The cell stretching technique used here is comprised of a weakly focused beam (which can be multiplexed to stretch cells in parallel) to stretch the sample along the beam axis. Stretching cell(s) by light in this set up is based on fact that light carries momentum and is transferred to the sample (of different refractive index) when it passes through it. In case of cells, the momentum transfer primarily takes place at the surface. For the reason that cells are elastic, it is possible to stretch them by using these surface forces along the beam axis. Because the cells have higher refractive index as compared to surrounding medium, passing light through them will cause reflection and refraction at the interface. The direction and velocity of light travelling through the sample changes and so does its momentum. Since momentum is conserved, some of the momentum is transferred from light to the interface and thus force is exerted on the surface.

Let us consider a ray of light is passing through an assembly having 3 medium with refractive indices $n_1$, $n_2$ and $n_3$ as shown in Figure 3-1. Note that $n_1 > n_2 > n_3$. When a ray of light enters the part of assembly having refractive index $n_1$, light gains momentum according to Minkowski's theory [49]. Since momentum is conserved, it is compensated by recoiling of the medium. Thus total momentum is conserved. When light enters from $n_1$ to $n_2$, there is loss in momentum. This loss is compensated by gaining the surface momentum in the direction of light propagation. Similarly $2^{nd}$ surface will gain momentum

in the direction of the light propagation. Thus the total force acting on the cell is in the direction of light propagation leading to optical stretching of the cell.

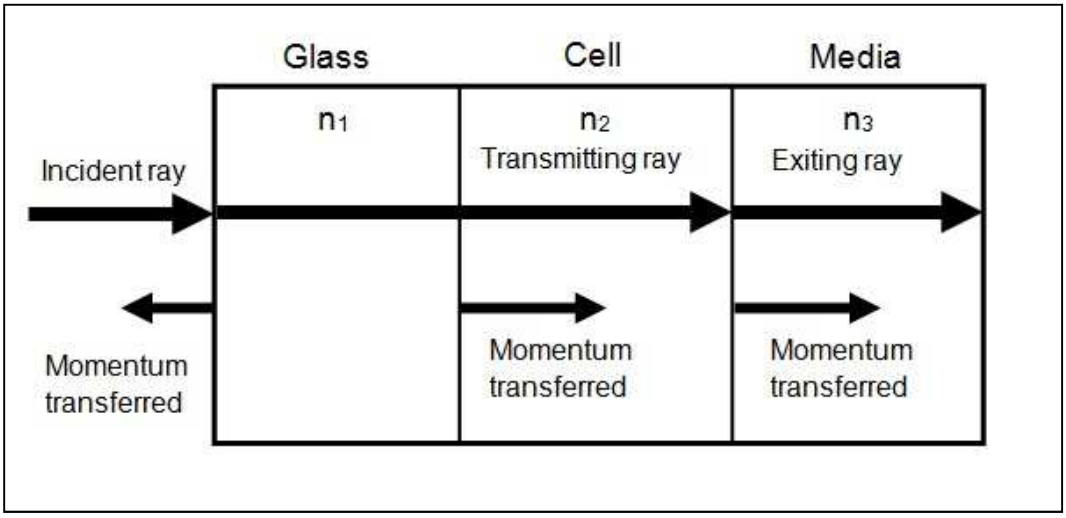


Figure 3-1: Momentum transfer and thus force acting on surfaces for light propagation through an assembly of different refractive indices.

Force acting on the cell membrane adhered to glass are of the order of pico-Newtons [35]. This force is negligible as compared to the force of adhesion of cells on to glass coverslip. Thus effective force acting on the cell to stretch it is on its outer surface and is in the direction of propagation of light.

## 3.2 Methods

Figure 3-2 shows the setup for stretching cells optically by using one beam. The setup consists of imaging laser set at 980nm. A condenser concentrates the beam on the sample placed on X-Y translational stage. The setup uses common path interferometric technique for NIR quantitative phase imaging. The setup is similar to NIR QPM setup except the fact that another laser is incorporated for optically stretching the cells. The stretching laser is a Ti: Sapphire laser set to stretch at 830nm. A dichroic mirror placed in front of the laser that reflects wavelengths below 850nm when placed at 45 degrees. The

light transmitted from the sample is passed through the dichroic mirror and the stretching laser is reflected off the mirror.

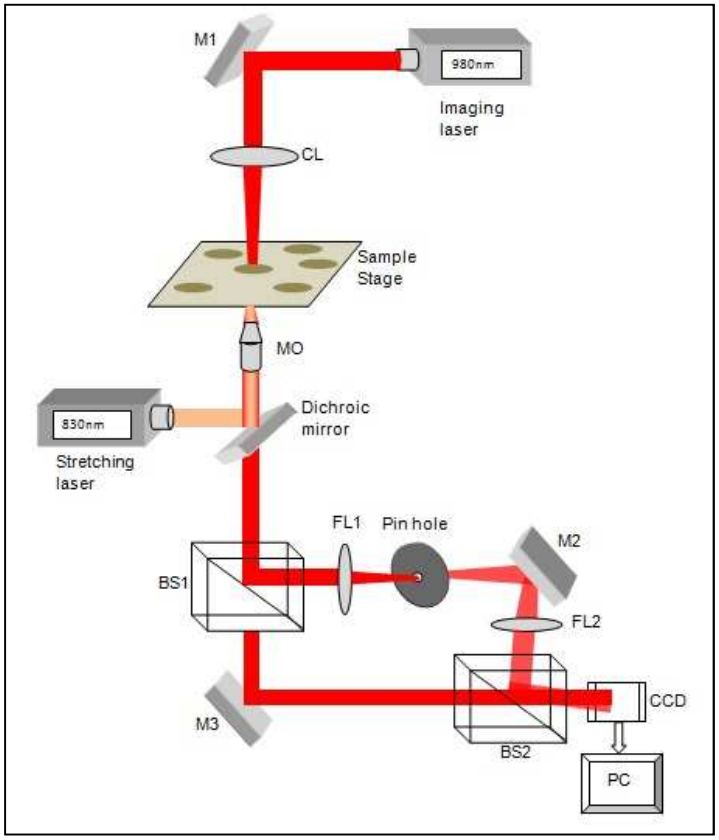


Figure 3-2: Optical stretching setup combined with NIR QPM.

For optically stretching the cells, the stretching laser is passed through the back aperture of microscopic objective (40X) having N.A. of 0.6 and is focused well above the cell to have the light weakly focused as shown in the Figure 3-3. Weakly focusing of light allows controlled selective stretching of a cell area.

As shown in the Figure 3-3, the laser focus is above the imaging plane. This configuration applies force on the cell membrane which is not attached to the glass coverslip over a selective area and thus stretching the cell optically along the beam axis. Although the stretching laser has Gaussian profile, since it is weakly focused, the

Gaussian profile is spread over the area of ~700 $\mu m^2$ at imaging plane. Hence, here we hypothesize that the Gaussian profile is flattened over its peak. The stretching laser has a diameter of 30 µm at the sample plane.

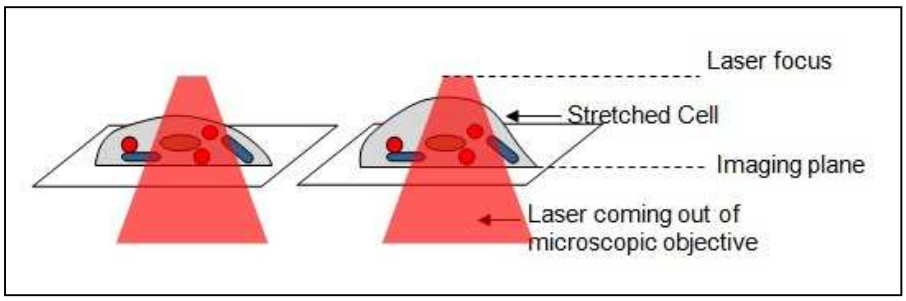


Figure 3-3: Illustration of optical stretching of a cell attached on a glass coverslip. Laser focus is above the imaging plane.

As shown in Figure 3-4, the stretching laser focus distance from imaging plane (h) is calculated by using simple geometry. Numerical aperture of microscopic objective used is 0.6. Therefore θ= 36.87º, and x=15 µm (radius of laser spot at imaging plane). Now $\tan(\theta) = {}^{x}/_{h}$. Hence h= 20 µm.

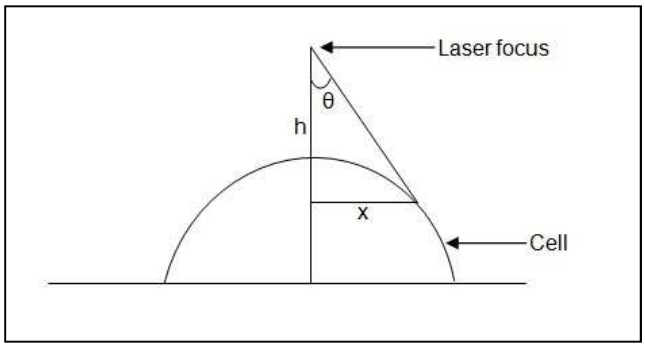


Figure 3-4: Calculation of stretching laser focus distance from imaging plane.

Normal HEK cells and HOX-B9 over expressed HEK cells are studied for their elasticity by optically stretching them using the setup described above. All the cells are grown in a glass bottom Petri dish in an incubator at 37ºC and are attached to the glass

coverslip. Phase images are recorded before and during the optical stretching. All the cells are imaged by a 40X microscopic objective having N.A. of 0.6.

## 3.3 Results and Discussion

Optical phase of a cell depends on its integral refractive index and its thickness. Thickness of a cell can be changed by exposing a cell to a mechanical force arising from its external environment. The integral refractive index of the cell remains unchanged. This change in thickness can be seen as increased phase shift of optical waves passing through the cell. Thus change in optical phase shift is an indicator of change in cell thickness due to optical stretching of the cell. Studying this change in optical phase shift can unravel a cell's elasticity. A cell having less viscosity will have more phase change than the one which is more elastic.

### *3.3.1 Optical stretching of HEK Cells*

Bright field images showing interference fringes over normal HEK cells are shown in Figure 3-5 (a). As phase of the image is contained in the fringe information, $1^{st}$ order of FFT of the bright field image is selected as shown in Figure 3-5 (b). The inverse Fourier transform of the selected $1^{st}$ order give the phase information contained in the cell. The phase image is unwrapped in a Matlab® program giving a 2D unwrapped image showing phase values of the cell. The cell is then stretched by stretching laser having wavelength 830nm at 150mW power measured after microscopic objective.. Stretching laser is passed through the back aperture of microscopic objective which is then focused above the sample to obtain weakly focusing beam passing through the sample.

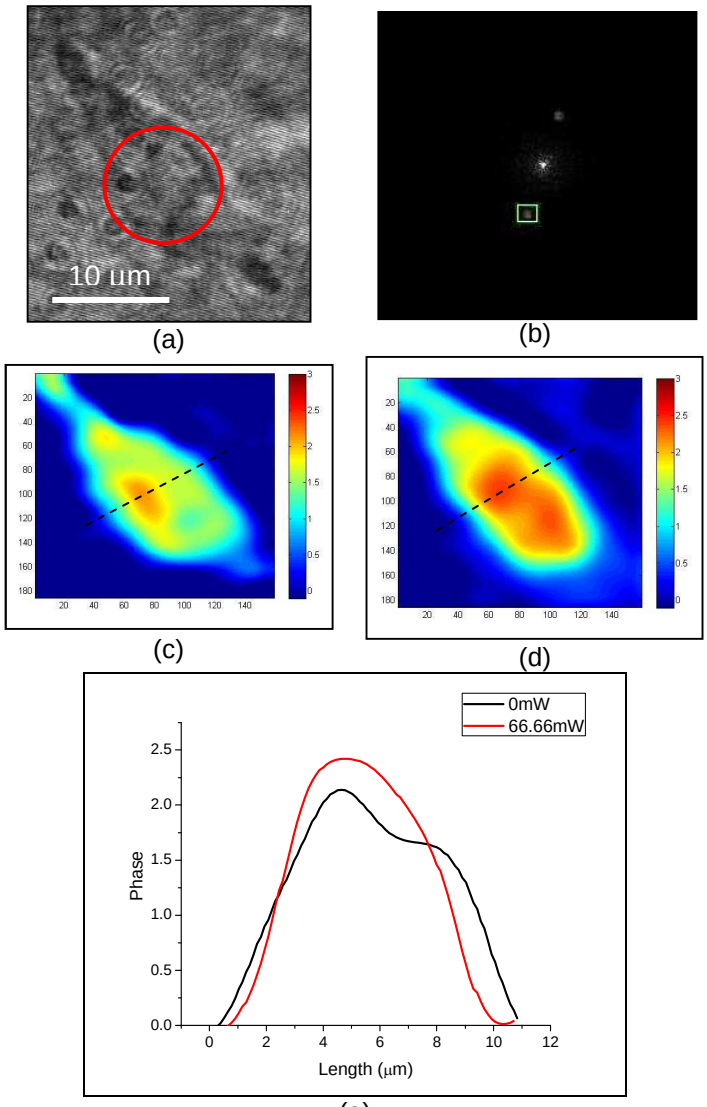


Figure 3-5: Optical stretching of normal HEK cell (a) Bright field image of a HEK cell. (b) FFT of the bright field image and selection of 1st order. (c) Unwrapped image of HEK cell before optically stretching showing a line on which phase profile was taken. (d) Unwrapped image of a HEK cell being stretched showing a line on which phase profile is taken. (e) Phase profile for control (cell without stretching) and 66.66 mW (Cell under 66.66 mW of stretching beam) over a line selected on unwrapped image.

Phase unwrapped image of the cell being stretched is shown in Figure 3-5 (d). A significant change in phase values can be observed when images of the cell before and after stretching are compared. A phase profile over a line is obtained as shown in Figure 3-5 (e). Graph shows that there is considerable mean phase change (0.3057) along the phase profile of the cell in the beam propagation direction. Moreover the length of cell is also decreased because of upward stretching. The phase change is due to change in cell's thickness along the direction of the beam. The force exerted on the cell wall pushes the membrane in the direction of the beam increasing the total thickness of a cell.

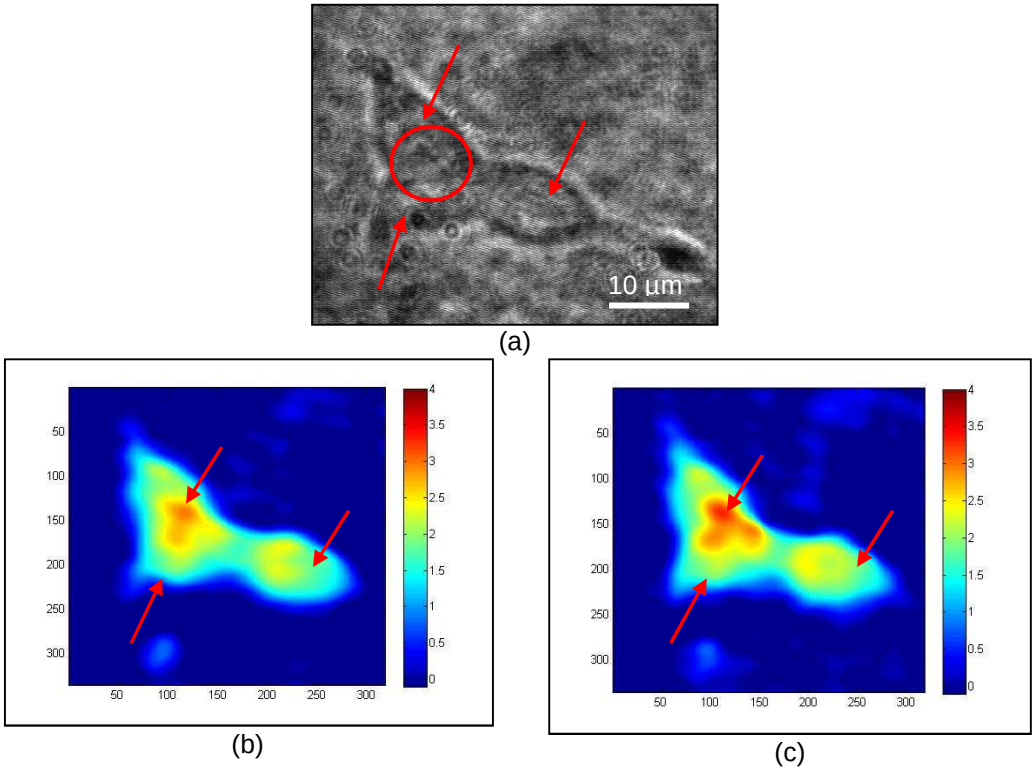


Figure 3-6: Optical stretching of 3 normal HEK cells (a) Bright field image of 3 cells marked with arrows showing the stretching beam position marked by a circle (b) Unwrapped image of 3 HEK cells with no stretching beam (c) Unwrapped image of 3 HEK cells under the influence of stretching beam showing higher increase in phase for 2 cells.

To see the effect of the stretcher onto neighboring cells, three cells attached together are stretched at a particular position as shown by a circle in Figure 3-6. Figure 3-6 (a) shows three cells marked with arrows and stretching laser spot marked by a circle kept on two cells. Phase unwrapped image of the cells before stretching is shown in Figure 3-6(b). During stretching as shown in Figure 3-6(c), the part exposed directly to laser spot got stretched more as compared to cell which is not placed directly at the laser spot. There is a slight change in phase difference for 3$^{rd}$ cell though as marked by an arrow. A total of 5 normal HEK cells were examined for elasticity measurement by optically stretching them. Mean phase change value ($\Delta\varphi$) shown by cells is 0.25 $\pm$0.05.

*3.3.2 Optical Stretching of HOX-B9 over-expressed HEK cells*

HOX-B9 over-expressed cells used here are tagged with GFP as shown in Figure 3-7. Cells showing fluorescence are recognized as HOX-B9 over-expressive cells and are used for stretching optically.

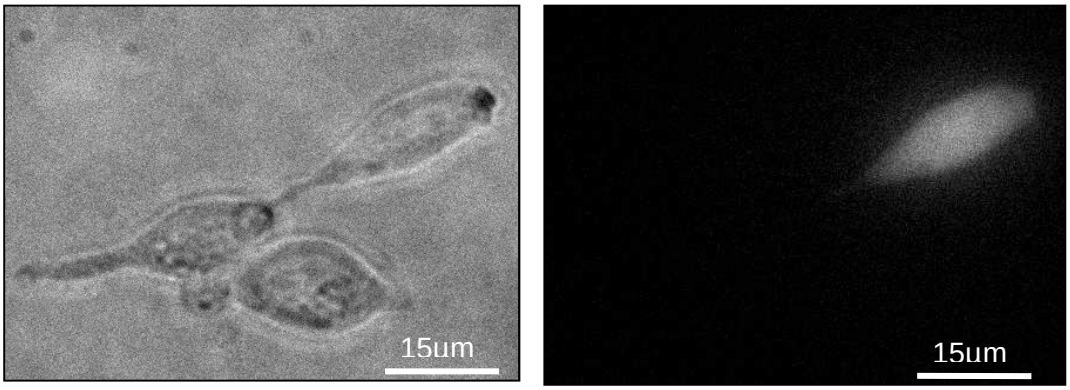


(a) (b)

Figure 3-7: HOX-B9 over expression tagged by GFP (a) Bright field image of HEK cells. HOX-B9 over-expressed cells are GFP tagged (b) Fluorescent image showing HOX-B9 over-expressed cell tagged with GFP.

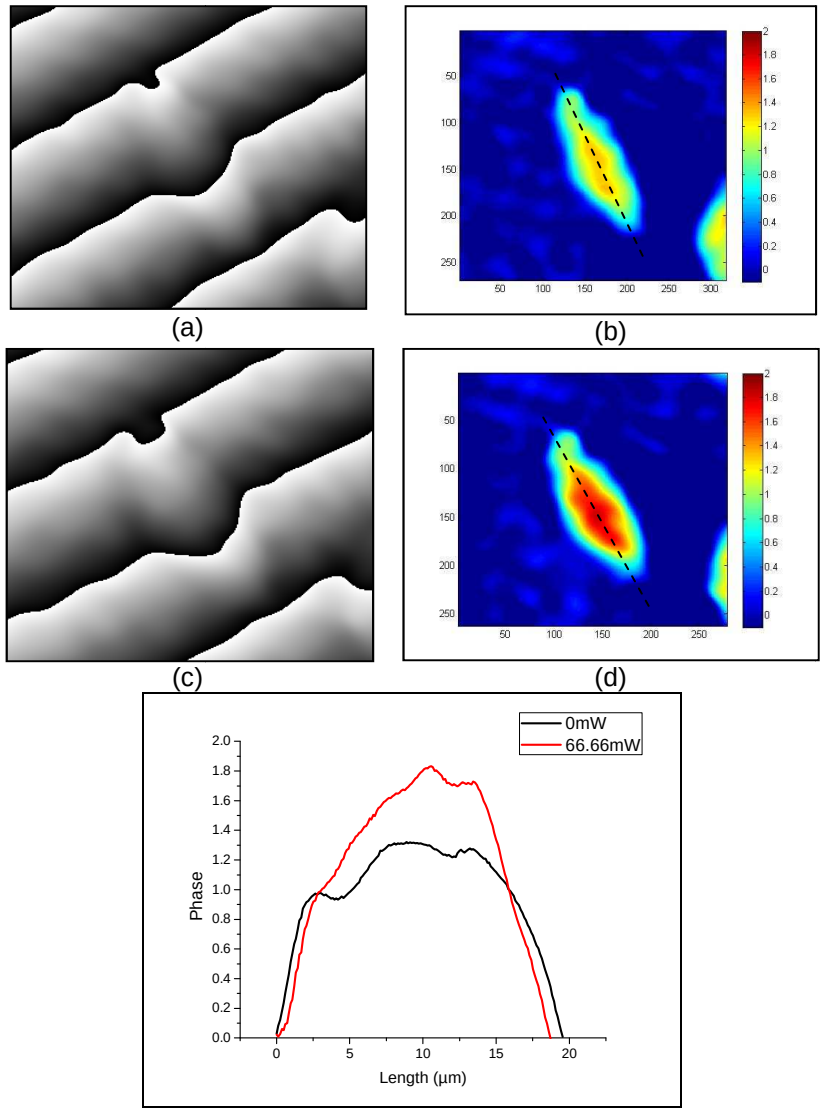


Figure 3-8: Comparison of HOX-B9 over expressed HEK cell with and without stretching (a) Phase wrapped image for non stretched HOX-B9 over expressive HEK cell. (b) Phase unwrapped image of non stretched HOX-B9 over expressive HEK cell. (c) Phase wrapped image of stretched HOX-B9 over expressive HEK cell at 66.66mW. (d) Phase unwrapped image for HOX-B9 over expressive HEK cell at 66.66mW. (e) Graph showing comparison of stretched cell with normal cell and difference in phase for the cell when stretched optically.

Figure 3-8 above shows a HOX-B9 over expressed cell being stretched at 150mW by a Ti: Sapphire laser having wavelength 830nm. Figure 3-8 (a) shows phase wrapped image and Figure 3-8 (b) shows unwrapped image of a HOX-B9 over expressed cell without stretching. After images are acquired for the cell without being stretched, laser beam is switched on and laser spot is kept on the cell. Figure 3-8 (d) shows unwrapped image of HOX-B9 over-expressed cell being stretched. When compared to image of cell without stretching, a significant difference in phase value of the cell is observed. For the cell shown in Figure 3-8, mean change in phase ($\Delta\varphi$) is 0.3397. Figure 3-8 (e) shows plot of phase profile taken over a line across the length of the cell as shown in Figure 3-8 (b) and (d). From the graph, it can be seen that there is significant amount of change in phase when the cell is stretched.

A total of five HOX-B9 over-expressed HEK cells are stretched optically. All the cells are stretched using Ti: Sapphire laser having wavelength 830 nm at 66.66mW. A 40X objective having NA of 0.6 is used to put cell membrane under laser pressure to optically stretch them. HOX-B9 over-expressed HEK cells showed a phase change value of 0.33 $\pm$0.03. Comparison of mean phase change value obtained for HOX-B9 over-expressed HEK cells to normal HEK cells revealed that HOX-B9 over-expressing HEK cells causes greater phase change when subjected to same stretching force (same laser power: 150 mW) as compared to normal HEK cells.

## 3.4 Young's Modulus

Young's modulus is a measure of stiffness of elastic materials. To calculate cell's elasticity and to compare normal HEK cells to HOX-B9 over-expressed HEK cells, young's modulus is calculated for both the types of cells.

*3.4.1 Calculation of force on the cell membrane*

The total power of the laser spot at imaging plane is 150 mW. Since the laser spot has a diameter of 30 µm, it is necessary to calculate effective power incident on the cell. We hypothesize that the laser beam has a uniform intensity profile at its center. Moreover a cell is assumed as a semi-sphere having radius of 10 µm. Thus total power incident on the cell is given by

$$P_{cell} = \frac{P_i \ \pi \ r_{cell}^2}{\pi \ r_{spot}^2} \tag{3-1}$$

Where, $P_i$ is total power incident, $r_{cell}$ and $r_{spot}$ are radius of cell and laser spot at imaging plane respectively. The total laser power incident on cell is 66.666mW that is ~66.67mW.

In the setup described above, cells are getting stretched because of force of incident laser beam on cell's top membrane which is not attached to glass coverslip. When light travels through cell to its surrounding media, the momentum decreases and this decrease in momentum is compensated by momentum transferred to cell membrane. The momentum transferred to the membrane applies a force on the cell membrane in the direction of light propagation. At normal incidence ($\theta$ = 0º) only fraction of the light (0.06%) is reflected at the interface for cell having normal refractive index ($n_{cell}$) of 1.4 and that of surrounding medium is ($n_{media}$) 1.33. The intensity reflection coefficient can be obtained as

$$\Gamma = \left( \frac{n_{cell} - n_{media}}{n_{cell} + n_{media}} \right)^2 \tag{3-2}$$

The momentum is given by m= n.p/c, where n is refractive index, p is energy of photons and c is speed of light in vacuum. Thus to calculate force applied on top surface of cell, we calculate force applied on every individual component. Product of refractive

index of cell ($n_{cell}$), transmission coefficient from glass to cell ($T_1$) and $P_{cell}$ gives us total power incident on cell.

$$F = \left[ n_{cell} \right] (T_1) \frac{P_{cell}}{c} \tag{3-3}$$

As light travels from cell to media, its momentum decreases and total force can be given by

$$F = \left[ T_2 . n_{media} \right] (T_1) \frac{P_{cell}}{c} \tag{3-4}$$

Hence we subtract product of transmission from cell to media and refractive index of media. There is also small amount of reflection at the boundary of cell and media and can be stated as,

$$F = \left[ (1 - T_2) n_{cell} \right] (T_1) \frac{P_{cell}}{c} \tag{3-5}$$

Because the net change in momentum is because of decrease in momentum when light travels from cell to media and its reflection form cell's top surface, we add the term ($1-T_2$) $n_{cell}$. Thus, the applied force on the cell top membrane can be calculated by using following formula.

$$F_{top} = \left[ n_{cell} - T_2 . n_{media} + (1 - T_2) n_{cell} \right] (T_1) \frac{P_{cell}}{c} \tag{3-6}$$

Where, $T_1$ is transmission coefficient glass to cell, $T_2$ is transmission coefficient from cell to media and c is speed of light in vacuum. $F_{top}$, the force applied on the top membrane of the cell is 17.04 pN for $P_{cell}$ of 66.67 mW.

*3.4.2 Calculation of strain*

Original thickness of normal HEK cell area and HOX-B9 over-expressed HEK cell area on which stretching occurred is calculated using the equation (2- 5) described in

chapter 2. Cell thickness is also obtained for stretched cells. Table 3-1 shows calculated cell length in the direction of light propagation for normal HEK and HOX-B9 over expressed HEK cells.

Table 3-1 Original length, stretched length and change in length for HEK and HOX-B9 over expressed HEK cells

| Cell | | 1 | 2 | 3 | 4 | 5 | Mean | SD |
|---|---|---|---|---|---|---|---|---|
| HEK | Original length (L) (µm) | 4.64 | 6.26 | 4.01 | 3.78 | 3.44 | 4.42 | 1.15 |
| | Stretched length (l) (µm) | 5.18 | 6.77 | 4.69 | 4.42 | 3.83 | 4.97 | 1.11 |
| | Difference (ΔL) (µm) | 0.54 | 0.51 | 0.68 | 0.64 | 0.39 | 0.55 | 0.11 |
| HOX-B9 Over expressed HEK | Original length (L) (µm) | 3.2 | 4.78 | 2.26 | 6.6 | 5.44 | 4.45 | 1.73 |
| | Stretched length (l) (µm) | 3.9 | 5.49 | 3.01 | 7.48 | 6.15 | 5.2 | 1.77 |
| | Difference (ΔL) (µm) | 0.7 | 0.71 | 0.75 | 0.88 | 0.71 | 0.75 | 0.07 |

Figure 3-9 shows graph of change in length of HEK cells compared to HOX-B9 over expressed HEK cells. From the graph, it is clear that HOX-B9 over expressed HEK cell shows more stretching for the same power level of 66.66 mW. Difference in stretched length is observed to be 230 nm. A t-test performed on the change of length shows p value of 0.003 implying statistically significant difference.

Strain which is defined as ΔL/L is calculated for every cell and mean is taken. Strain value for normal HEK cells is 0.131 and that of HOX-B9 over-expressed HEK cells is 0.194.

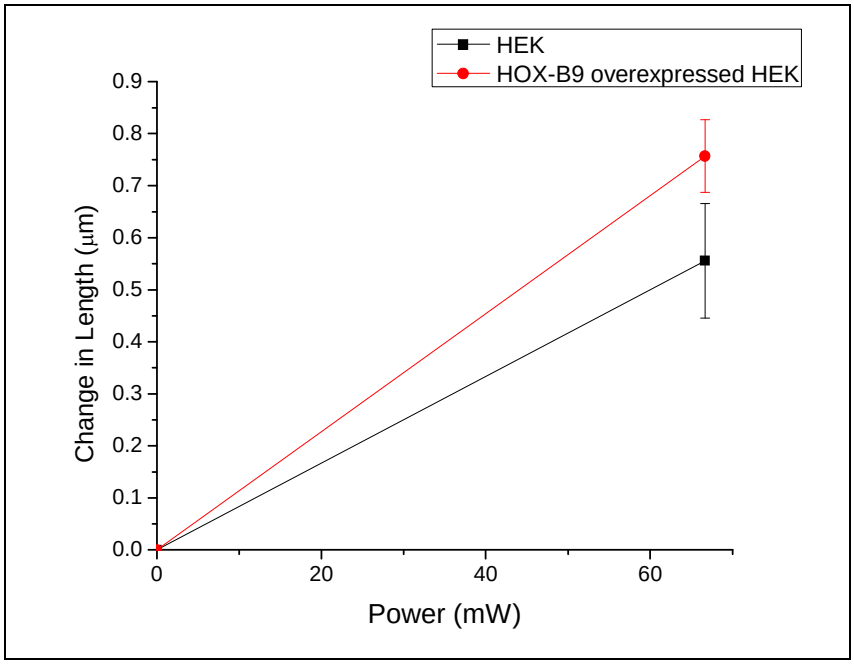


Figure 3-9 Change in cell length along the direction of laser for normal HEK cells and HOX-B9 over expressed HEK cells for laser power of 150mW.

*3.4.3 Calculation of Young's Modulus*

Young's modulus can be defined as Stress/Strain. Stress is force per area. Thus formula for young's modulus can be stated as follows.

$$Y = \frac{F/A}{\Delta L/L} \tag{3-7}$$

Young's modulus for normal HEK cells (Y) is 0.407 Pa and that of HOX-B9 over expressed HEK cells is 0.274 Pa. Malignant cells have shown lower magnitude of young's modulus number than normal healthy cells [44]. HOX-B9 over expression in breast cancer cells have shown to support tumorigenesis. Moreover over expression of this protein can be a potential contributor towards tumorigenesis in HEK cells as well [51]. Results here show that HOX-B9 over-expressed HEK cells stretch more than normal HEK cells for constant laser power of 150mW. In addition to this, young's modulus which is a measure of stiffness is less for HOX-B9 over-expressed HEK cells than normal HEK cells support the fact that over-expression of HOX-B9 in HEK cells leads to tumor progression.

Table 3-2 below shows comparison of various cell stretching techniques, their advantages, limitations and imaging resolution.

Table 3-2: Comparison of various cell stretching techniques

| Method | Advantages | Limitations | Imaging resolution |
|---|---|---|---|
| Atomic Force Microscopy | Can give topographic images of sample | Needs contact of tip on cells and could give false results | 1nm laterally & 0.1 nm axially |
| Optical Tweezers | Stretches laterally by optically trapping beads attached on cells | Needs perfect attachment of beads to cells, time consuming | 100 nm |
| Micropipette Aspiration | Uses a micropipette to apply negative pressure on cell, Simple to use | Contact of micropipette tip on cell is necessary | 25 nm |

Table 3-2—*Continued*

| | | | |
|---|---|---|---|
| Optical Stretching in accordance with DHM | Does not need attachment of any kind onto cells for stretching, stretches in the direction of light | Need high power defocused beam for large optical stretching | Angstrom |

# Chapter 4

## Conclusions and Future Scope

The thesis demonstrates novel use of NIR QPM for cell investigations under silicon. DHM using NIR light to see through opaque silicon and characterize samples under it can be used to obtain nanometer precision quantitative information about samples. The specific wavelength used in this thesis for imaging samples through silicon is optimized on the basis of results obtained from transmission through silicon, fringe contrast dependence taking into consideration the sensitivity of silicon based CMOS camera. DHM has also shown to reveal shape, refractive index and thickness of samples under silicon wafer. For example, thickness and disc shape of RBCs underlying silicon wafer, refractive index of polystyrene particles are explored. Use of DHM under silicon environment in quantifying cell characteristics undergoing hypotonic stimulation is explored. As shown by DHM imaging of cells under silicon exposed to hypotonic stimulation, there is net decrease in cell's phase which mostly contributes towards cell's integral refractive index, although hypotonic shock is meant to increase cell's thickness by inducing water influx. This change in cell's phase and thus in refractive index is due to dissolved proteins inside cell which mainly contributes to integral refractive index of a cell.

As a future scope; to image cells through thick silicon wafer by using NIR QPM, higher wavelengths usually greater than 1100nm can be used. As silicon have higher transparency at higher wavelengths, using higher wavelengths would definitely improve imaging through silicon in various silicon based micro devices that may not have restrictions on thickness of silicon substrate. In addition to this, incorporation of Infrared camera instead of silicon based CMOS camera could improve on fringe contrast thus improving image quality. Moreover, different types of cell's interaction with each other or

to a different chemical or drug can be studied by DHM while obtaining simultaneous results on electrical activity going on in cells by silicon based micro devices.

This thesis also describes an innovative method by which cells are optically stretched in the direction of light propagation. Force applied on cell's top surface is calculated from an empirical formula developed using first order assumptions. The cell under consideration is assumed to be semi-sphere with radius of 10 μm. Light transmission from glass to cell is 100% as reflection from glass surface is less than 0.02%. Cell's refractive index is taken to be 1.40 and that of media is assumed to be 1.33. Elasticity of cells is calculated by obtaining Young's modulus. Tests are performed on normal HEK cells and HOX-B9 over expressive HEK cells to see if over expression of HOX-B9 protein alters cellular viscoelastic properties. To our findings, Young's modulus for HEK cells is greater than that of HOX-B9 over expressed HEK cells implying HOX-B9 over expressed HEK cells are softer and can be stretched more as compared to normal HEK cells. This proves that over expression of HOX-B9 protein in HEK cells could be a contributor towards transformation of healthy cells into a malignant one.

The calculated force measurements can be precisely done on symmetrically shaped RBCs. This will allow high throughput measurement of alteration in RBC elasticity due to malaria parasite invasion. However, new modeling of force based on cell shape and ref index distribution is required for other non-symmetrically shaped cells. While shape can be determined using DHM with known refractive index, the refractive index distribution can be determined using tomographic phase microscopy. Further, temporal relaxation of stretched cell can be monitored for measurement of viscoelastic time constant.

# Appendix A

## Abbreviations

NIR: Near Infrared

QPM: Quantitative Phase Microscopy

DHM: Digital Holographic Microscopy

PCM: Phase Contrast Microscopy

DIC: Differential Interference Microscopy

HMC: Hoffman Modulation Contrast

HEK: Human Embryonic Kidney

References

[1] R. P. Carlisle, Scientific American Inventions and Discoveries: All the Milestones in Ingenuity—from the Discovery of Fire to the Invention of the Microwave Oven (John Wiley & Sons, Hoboken, N, 2004).

[2] Milestones in light microscopy*, Nat Cell Biol*, 11, 1165–1165 (2009).

[3] DiBona DR, Kirk KL, Johnson RD. Microscopic investigation of structure and function in living epithelial tissues. FASEB Fed. Proc. 1985; 44:2693-2703.

[4] The Abbe theory of imaging: an alternative derivation of the resolution limit. 1986 Eur. J. Phys. 7 62.

[5] An Introduction to Electron Microscopy. FEI™ ISBN 978-0-578-06276-1.

[6] Martin Chalfie, Yuan Tu, Ghia Euskirchen, William W. Ward, Douglas C. Prasher: Green Fluorescent Protein as a Marker for Gene Expression. Science . Vol. 263 . 11 FEBRUARY 1994

[7] David Huang; Eric A. Swanson; Charles P. Lin; Joel S. Schuman; William G. Stinson; Warren Chang; Michael R. Hee; Thomas Flotte; Kenton Gregory; Carmen A. Puliafito; James G. Fujimoto: Optical Coherence Tomography. Science, New Series, Vol. 254, No. 5035 (Nov. 22, 1991), 1178-1181.

[8] Judith A. Drazba: Introduction to Confocal Microscopy. Microsc Microanal 12(Supp 2), 2006.

[9] C. Maurer, A. Jesacher, S. Bernet, and M. Ritsch-Marte: Phase contrast microscopy with full numerical aperture illumination Opt.Express 16, 19821 (2008).

[10] Zernike F. Phase-contrast, a new method for microscopic observation of transparent objects. Part I. Physica 9: 686-698, 1942.

[11] M.R. Arnison, K. G. Larkin, C. J. R. Sheppard, N. I. Smith, C. J. Cogswell: Linear phase imaging using differential interference contrast microscopy, Journal of microscopy, Vol. 214, pt 1 April 2004, pp.7-12

[12] Robert Hoffman and Leo Gross: Modulation Contrast Microscope. Applied Optics, Vol. 14, Issue 5, pp. 1169-1176 (1975)

[13] Hoffman R & Gross L. The modulation contrast microscope. Nature. 1975; 254:586-588.

[14] Barer R. Refractometry and interferometry of living cells. J. Opt. Soc. Am. 1957; 47:545-556.

[15] Paganin D & Nugent KA. Non-interferometric phase imaging with partially coherent light. Phys. Rev. Lett. 1998; 80:2586-2589.

[16] Barone-Nugent ED, Barty A, Nugent KA. Quantitative phase-amplitude microscopy I: optical microscopy. J. Microsc. 2002; 206:194-203.

[17] William Mason Ash: Total internal reflection holographic microscopy (TIRHM) for quantitative phase characterization of cell-substrate adhesion, University of South Florida Scholar Commons Theses and Dissertations

[18] Pierre Marquet, Pierre J. Magistretti, Benjamin Rappaz, Tristan Colomb, Jonas Kühn, Christian Depeursinge: Quantitative Measurements of Dynamic Cell Morphometry and Intracellular Integral Refractive Index with Digital Holographic Microscopy. @2006 Optical Society of America OCIS codes: (090.0090) Holography; (180.3170) Interference microscopy; (170.1530) Cell analysis

[19] Pierre Marquet, Benjamin Rappaz, Pierre J. Magistretti, Etienne Cuche, Yves Emery,Tristan Colomb, and Christian Depeursinge: Digital holographic microscopy: a noninvasive contrast imaging technique allowing quantitative

visualization of living cells with subwavelength axial accuracy, Optics Letters, Vol. 30, Issue 5, pp. 468-470 (2005)

[20] Claire L. Curl, Catherine J. Bellair, Peter J. Harris, Brendan E. Allman, Ann Roberts, Keith A. Nugent & Lea M.D. Delbridge: Quantitative phase microscopy – a new tool for investigating the structure and function of unstained live cells, Proceedings of the Australian Physiological and Pharmacological Society (2004) 34: 121-127

[21] Lingfeng Yu, Samarendra Mohanty, Jun Zhang, Suzanne Genc, Myung K. Kim, Michael W. Berns, and Zhongping Chen: Digital holographic microscopy for quantitative cell dynamic evaluation during laser microsurgery. Opt Express. 2009 July 6; 17(14): 12031–12038.

[22] Yong-Seok Choi and Sang-Joon Lee: Three-dimensional volumetric measurement of red blood cell motion using digital holographic microscopy. Applied Optics, Vol. 48, Issue 16, pp. 2983-2990 (2009).

[23] Gabriel Popescu: Quantitative Phase imaging of cells and tissues. McGRAW-HILL, Biophotonics

[24] Mitsuo Takeda, Hideki Ina and Seiji Kobayashi: Fourier-transform method of fringe-pattern analysis for computer-based topography and interferometry. J. Opt. Soc. Am./Vol. 72, No. 1/January 1982

[25] U. Schnars and W. Jüptner.: Direct recording of holograms by a CCD target and numerical reconstruction. Appl Opt. 1994 Jan 10;33(2):179-81. doi: 10.1364/AO.33.000179.

[26] Etienne Cuche, Pierre Marquet, and Christian Depeursinge: Simultaneous amplitude-contrast and quantitative phase-contrast microscopy by numerical

reconstruction of Fresnel off-axis holograms. Applied Optics, Vol. 38, Issue 34, pp. 6994-7001 (1999).

[27] Goldstein, R. M., Zebker, H. A. and Werner, C. L., “Satellite radar interferometry: Twodimensional phase unwrapping”, Radio Sci. 23, 713-720 (1988).

[28] Kersti Alm, Helena Cirenajwis, Lennart Gisselsson, Anette Gjo□rloff Wingren, Birgit Janicke, Anna Mo□lder, Stina Oredsson and Johan Persson (2011). Digital Holography and Cell Studies, Holography, Research and Technologies, Joseph Rosen (Ed.), ISBN: 978-953-307-227-2, InTech, Available from: http://www.intechopen.com/books/holography-research-and-technologies/digital-holography-and-cell-studies

[29] Bimbo, Luis M.; Sarparanta, Mirkka; Mäkilä, Ermei; Laaksonen, Timo;Laaksonen, Päivi; Salonen, Jarno; Linder, Markus B.; Hirvonen, Jouni;Airaksinen, Anu J., Santos, Hélder A. “Cellular interactions of surface modified nanoporous silicon particles”. Nanoscale, Volume 4, Issue 10, pp. 3184-3192 (2012).

[30] Elliot E. Hui and Sangeeta N. Bhatia. “Micromechanical control of cell–cell interactions”. PNAS April 3, 2007 vol. 104no. 14 5722-5726.

[31] M. Simion, I. Kleps, F. Craciunoiu, L. Savu, M. Miu, A. Bragaru. “Silicon chip technology - electrophoretic dna analisys” romanian journal of information science and technology volume 10, number 1, 2007, 35-41

[32] Geoffrey Kotzar, Mark Freas, Phillip Abel, Aaron Fleischman, Shuvo Roy, Christian Zorman, James M. Moran, Jeff Melzak. “Evaluation of MEMS materials of construction for implantable medical devices”. Elsevier Biomaterials 23 (2002) 2737–2750

[33] Oded Rabin, Paul R. Hertz, Yu-Ming Lin, Akintunde I. Akinwande, Stephen B. Cronin and Mildred S. Dresselhaus. “ Formation of thick porous anodic alumina

films and nanowire arrays on silicon wafers and glass". Adv. Funct. Mater. 2003, 13, No. 8, August

[34] Soo-Kng Teo, Andrew B. Goryachev,Kim H. Parker, and K.-H. Chiam. : Cellular deformation and intracellular stress propagation during optical stretching. PHYSICAL REVIEW E 81, 051924 _2010.

[35] Jochen Guck, Revathi Ananthakrishnan, Hamid Mahmood, Tess J. Moon, C. Casey Cunningham, and Josef Kas : The Optical Stretcher: A Novel Laser Tool to Micromanipulate Cells. Biophysical Journal Volume 81 August 2001 767–784.

[36] Sui Huang & Donald E. Ingber : The structural and mechanical complexity of cell-growth control. Nature Cell Biology 1, E131 - E138 (1999) doi:10.1038/13043.

[37] Hayden Huang, Roger D. Kamm, and Richard T. Lee : Cell mechanics and mechanotransduction: pathways, probes, and physiology . Am. J. Physiol.: Cell Physiol. 287, C1 _2004.

[38] N. Wang, D.E. Ingber: Control of cytoskeletal mechanics by extracellular matrix, cell shape, and mechanical tension. Biophys. J. 66, 2181 _1994.

[39] X. J. Liang, A. Q. Liu, C. S. Lim, T. C. Ayi, and P. H. Yap, "Determining refractive index of single living cell using an integrated microchip," Sensor. Actuat. A: Physical, 133(2), 349-354 (2007).

[40] K. Hoyt, B. Castaneda, M. Zhang, P. Nigwekar, P. A. di Sant'agnese, J. V. Joseph, J. Strang, D. J. Rubens, and K. J. Parker, "Tissue elasticity properties as biomarkers for prostate cancer," Cancer Biomark, 4(4-5), 213-25 (2008).

[41] T. A. Krouskop, T. M. Wheeler, F. Kallel, B. S. Garra, and T. Hall, "Elastic moduli of breast and prostate tissues under compression," Ultrason Imaging, 20(4), 260-74 (1998).

[42] R. P. Jagannath, and P. K. Yalavarthy, “Approximation of internal refractive index variation improves image guided diffuse optical tomography of breast,” IEEE Trans. Biomed. Eng., 57(10), 2560-3 (2010).

[43] Olivier Thoumine, Albrecht Ott : Comparison of the mechanical properties of normal and transformed fibroblasts. Biorheology 34, 309 1997.

[44] R. E. Mahaffy, C. K. Shih, F. C. MacKintosh and J. Käs : Scanning Probe-Based Frequency-Dependent Microrheology of Polymer Gels and Biological Cells. Phys. Rev. Lett. 85, 880 (2000)

[45] M. Lekka, P. Laidler, D. Gil, J. Lekki, Z. Stachura and A. Z. Hrynkiewicz: “Elasticity of normal and cancerous human bladder cells studied by scanning force microscopy.” EUROPEAN BIOPHYSICS JOURNAL Volume 28, Number 4 (1999), 312-316

[46] K. A. Ward, W. Li, S. Zimmer, and T. Davis: Viscoelastic properties of transformed cells: role in tumor cell progression and metastasis formation. Biorheology 28, 301 (1991)

[47] C.T. Lim, M. Dao, S. Suresh , C.H. Sow , K.T. Chew: Large deformation of living cells using laser traps. Acta Materialia 52 (2004) 1837–1845

[48] Hiroaki Kojima, Etsuko Muto, Hideo Higuchi, and Toshio Yanagida : Mechanics of Single Kinesin Molecules Measured by Optical Trapping Nanometry. Biophysical Journal Volume 73 October 1997 2012-2022

[49] Stephen M. Barnett. : Resolution of the Abraham-Minkowski Dilemma. Physical Review Letters (2010) 104, 070401

[50] Hayashida T, Takahashi F, Chiba N, Brachtel E, Takahashi M, Godin-Heymann N, Gross KW, Vivanco MM, Wijendran V, Shioda T, Sgroi D, Donahoe PK,Maheswaran S “HOXB9, a gene overexpressed in breast cancer, promotes

tumorigenicity and lung metastasis.” Proc Natl Acad Sci U S A. 2010 Jan 19;107(3):1100-5. Epub 2009 Dec 28.

[51] Bishakha Shrestha, Khairul I. Ansari, Arunoday Bhan, Sahba Kasiri, Imran Hussain and Subhrangsu S. Mandal. “Homeodomain-containing protein HOXB9 regulates expression of growth and angiogenic factors, facilitates tumor growth in vitro and is overexpressed in breast cancer tissue.” FEBS Journal Volume 279, Issue 19, Article first published online: 31 AUG 2012

## Biographical Information

Bipin Joshi earned a degree of Bachelor of Engineering in Biomedical Engineering from the University of Mumbai in the year 2009 securing first class with distinction. While studying his engineering, he worked at Wockhardt Hospitals Ltd. as a Biomedical engineer trainee for the duration of August 2008 – January 2009. He graduated from University of Mumbai earning his degree in Engineering after successfully completing his project on “Micro-controller based Temperature Meter” under the supervision of Dr. Sanghvi. Due to his aspiration to gain more knowledge in the area of Biomedical Engineering specifically in Optics, he gained an admission in University of Texas at Arlington in fall 2010.

He started working in Biophysics lab as a graduate student of Bioengineering to complete his thesis under the guidance of Dr. Mohanty at UT Arlington. He successfully graduated in the year 2012 by defending his MS thesis on “Near-Infrared Quantitative Phase Imaging of Cellular Manipulation under different Physio-Chemical environments”. While in his master’s curriculum, he worked as an intern in research and development department at Alcon research (Forth Worth, TX, USA). As an intern he completed two assigned projects in time and produced significant results. His future plans include working in the area of optics and Bioengineering to help making people lives better. All his academic interest lies in the areas of optics, Biophysics and Bioengineering.